

AD-A246 717



✓
①

ARATS: ROLE OF THE U.K. MET OFFICE LONG RANGE TRANSPORT MODEL.

3RD INTERIM REPORT, 24TH APRIL - 31ST DECEMBER 1991.

by

R.H.MARYON.



PRINCIPAL RESEARCH OFFICE OF THE U.S. ARMY

London, England.

Contract Number: DAJA45-90-C-0051.

~~92-01242~~
~~92-01242~~

92 2 25 214

~~92-1-15-034~~

1

92-04949



U.S. Army Regional Aerosol Transport Simulation (ARATS)

Contract DAJA45-90-C-0051: Third Interim Report.

Introduction.

The Second Interim Report concluded by identifying 3 possible lines of continuation:

1. The influence of synoptic type upon dispersion.
2. The stability of multi-particle models used for long range transports, and
3. Casework and model intercomparisons associated with events in the Gulf as determined in discussion with Dr Holt and other ARATS scientists.

However, the adventitious occurrence of the Gulf oil fire plume has led Dr Holt to redirect the main thrust of the investigation away from 1 and 2 and towards 3, that is, studies of the spread of pollutants from Kuwait using a range of numerical modelling techniques. At the 2nd ARATS Workshop it was agreed between Dr Holt, Dr ApSimon of Imperial College and myself representing the U.K. Met Office that the continuation and conclusion of the work under the existing contracts should take the form entirely of a comparative study of the numerical modelling of the plume during an interval when it was particularly well observed by aircraft and satellite, using Imperial College's '3-DRAW' model and the Met Office 'NAME' model. These are both long range transport models using multiple particle methods, but are differently structured and parametrized. A single data base is to be provided by the Met Office. Such a comparison should prove invaluable at highlighting those aspects of the dispersion parametrizations which can lead to significant differences in simulation.

This study will then, at Dr Holt's request (and perhaps also in recognition of the changing geopolitical scene), to replace the work on synoptic type over Europe. However, good progress had already been made on the 2nd of the above projects, a detailed study of the stability of the NAME model with respect to the particle numbers used. This gave a first assessment of the optimal particle numbers required by a 'Monte Carlo' multiple-particle model adequately to simulate the spread of a continental-scale plume over a period of a week to 10 days. This may well be the first time this has been attempted.

Under head 3 must be included the major Met Office contribution to the 2nd ARATS Workshop. A description is given below of the extensive modelling work carried out in preparation for this meeting, supplemented with more detail in Annexes, and of the Met Research Flight contribution.



Accession For	
NTIS	CRA&I
DTIC	TAB
Unannounced	
Justification	
By <i>[Signature]</i>	
Distribution/	
Availability Codes	
Dist	Avail. and/or Special
A-1	

The 2nd Workshop on the Army Regional Aerosol Transport Simulation-ARATS 2.

The success of this meeting owed much to the efforts of U.K. Met Office staff. The following attended:

Dr P W White, Deputy Director (Short-range Forecasting Research).

Dr F B Smith, senior Met Office dispersion scientist.

R H Maryon, Head of Special Investigations and Nuclear Accident Response.

Mrs S P Ballard, meso-scale NWP modelling.

D W Johnson, Met Research Flight.

On the first morning R Maryon and Mrs Ballard presented modelling studies of the Gulf oil fire plume for material released from 0000UCT on 1st March 1991: a case chosen in advance by Dr Holt. A description of the products of the meso-scale model was written up by Mrs Ballard and R T H Barnes (Annex 1), and sample output from the corresponding integrations of the NAME regional model provided by R Maryon (Annex 2). These models are complementary, the meso-scale handling the near-source plume which is interacting with the local meteorology, NAME the wider dispersion problem. NAME utilised analyses of the meteorology from the U.K. Met Office operational numerical weather prediction (NWP) models while the meso-scale model was only initialised therefrom, and proceeded to generate its own developments on the meso-scale.

Both the models simulated the plume well during the 48 hr integrations, as far as can be deduced from satellite observations. Both picked up the complex, 3-dimensional, sheared structure of the plume. The meso-scale model generated interesting meso-scale circulations, induced by the land/sea juxtaposition and by the effects of the absorption of solar radiation by the dense smoke. Cells of ascending air, capped by pyrocumulus, were forecast, in general agreement with satellite and aircraft observations. Such effects as the temperature drop beneath the smoke (due to its shielding effects), and general levels of concentration were reasonably well handled.

The NAME model, of course, is a regional-scale model, which does not provide the resolution or detailed physics of the meso-scale model. In particular, it has no parametrization to represent the interaction of the plume with the meteorology of the atmospheric boundary layer (ABL)—the usually turbulent region close to the surface. Aircraft and other observations revealed that the plume modified the ABL, reducing the turbulent energy available at low levels, and accordingly reducing the mixing of smoke into the ABL until the plume eventually became sufficiently diffuse to allow renewed penetration of solar radiation and generation of turbulent kinetic energy (TKE). The NAME model diagnoses an ABL depth, but always assumes that the ABL is well-mixed by TKE in daytime conditions, and accordingly spread material through the ABL from the start.

Despite this, the NAME model reproduced the 3-dimensional structure and spread of the plume into the wider field very well, and it was considered that the model pos-

essed value in (1) providing a benchmark simulation, as a reliable and tested regional scale model, and (2) in providing a Lagrangian (as opposed to Eulerian) approach to the problem of modelling the transport, spread and deposition of pollutants or obscurants. Unlike the meso-scale model the NAME model was able to provide predictions of the time-integrated concentrations in air ('dosage') and most importantly, of sedimentation of pollutants to the surface and of their washout by rain.

The lofting of smoke by the absorption of solar radiation was also modelled by the NAME model, but in a different way from the meso-scale model. As NAME is a Lagrangian multi-particle model, the heating of particles by the flux-divergence of solar radiation had to be computed, and the individual particles then lifted buoyantly to their equilibrium level. Output from the lofting run is distinguished in Annex 2 by the letter B. It will be noted that in comparison with the non-lofting run (labelled A) the air concentrations in the ABL are substantially reduced, and that in the upper layer (to 850 mb) somewhat increased. Dry deposition of carbon to the surface, and time-integrated air concentrations in the ABL are also reduced. The results—the lofting generally limited to about 1 km, except for insignificant quantities of material—are qualitatively similar to those of the Eulerian meso-scale model, and indeed, this mutual support enabled an early prediction in Browning et al (1991) that the stratosphere (and hence global climate) would not be threatened by lofted smoke.

A future study might well look at the nesting of the meso-scale and regional models, the former to handle the interactive plume near the source, the latter the spread of material further afield. A most interesting suggestion is the initialising of the regional model from the output of a prior integration of the meso-scale model.

On the first afternoon a presentation was made by D Johnson of the Met Research Flight (MRF), who participated in the MRF C130 aircraft traversals of the plume during March 1991. Measurements of the local met conditions, radiation, air and plume chemistry, cloud physics and aerosol were made using the comprehensive instrumentation of this aircraft. The near- and far-field structures of the plume were also elucidated: a fuller account is given in Johnson et al (1991) which, with Browning et al (1991), is appended at Annex 3 for convenience. D Johnson also provided the Working Group with a comprehensive and very useful summary of the flights (Gibbs et al 1991), not reproduced here.

With the exception of D Johnson all members of the Met Office party brought their varied experience and expertise to the discussion and recommendations which are set out in the conference report.

Stability of the multiple-particle model.

The stability of multi-particle models used for simulating the long range transport and dispersion of pollutants and obscurants (item 2 above) was addressed during the summer of 1991, after the heavy workload generated by the Gulf environmental crisis had receded. This study may have been unique in the scale of the integrations carried out on the NAME model to establish adequate 'validation' against which practicable, run-of-the-day model

configurations could be assessed. For instance, integrations were made in which 6000 particles/hr were released and carried by the model *every hour for 240 hours*, and their transport and diffusive spread simulated. In another case 12000 particles/hr were released for 72 consecutive hours, and the simulation continued up to 240 hr. Integrations such as these required many Mbytes of core, and the runs consumed up to 9 hr of CPU time on the Met Office Hitachi computer. No attempt has been made to cost these overheads!

Additional code was written and added to the model to carry out the extensive statistical analysis required, and the results were plotted by writing graphics routines for a Microvax computer and transferring the data between the systems. The results are unexciting, but of very considerable practical importance: it is valuable to have some idea of the optimal number of particles which should be released in a multi-particle model (a) to simulate a given situation as well as the model is capable of doing but (b) not to tie up computer storage and CPU time processing large numbers of particles which are adding very little to the accuracy of the simulation. The results showed that for a Chernobyl-scale incident there is not a great deal to be gained over the European domain from releasing more than 500 particles/hr, and extremely little improvement obtainable beyond 1000 particles/hr, when limitations in the model's diffusion parametrization probably put constraints upon the achievable accuracy.

Opportunity was taken to write up these results for the NATO/CCMS 19th International Technical Meeting on Air Pollution Modelling and its Application, held at Ierapetra, Crete, Sept 1991, in view of the desirability of communicating these results to the wider modelling fraternity. A copy of this paper (Maryon 1992) is at Annex 4.

Plans for remainder of Contract.

In discussions with Dr Holt and Dr ApSimon, Imperial College, it was agreed to complete the project with a detailed and structured comparison of Imperial College's 3-DRAW and the Met Office's NAME long range transport and dispersion models. The integrations would start at 0000UCT 27th March 1991—a period for which both satellite and aircraft observations of the Gulf plume are available. The models will use identical release profiles in time and space, and in source emission strength: this is, for some reason, an ideal that has not quite been attained hitherto. The output will consist of trajectory endpoints, ABL and elevated level concentrations of carbon in air, and wet and dry deposition of carbon to the surface. Data for this analysis is to be assembled and provided by R Maryon at the Met Office. Dr ApSimon's and her colleague Dr Lowles' more detailed proposals are at Annex 5. As discussed in the Introduction, a comparison of two similar but differently parametrized models using identical scenario and data should be particularly invaluable in highlighting areas of potential uncertainty and difficulty in this type of simulation.

The relevance of this work to ARATS lies not only in the assessment of the suitability of models of this type for application in practical situations, and the reliance which can be placed upon their products, but also in the insights which can be gained into areas where the models have the potentiality of improvement. It is hoped that the results of this study will be available by the end of March next.

REFERENCES:

- Browning, K.A et al** including the present author (1991): 'Environmental effects from burning oil wells in Kuwait', London: *Nature* Vol 351, No 6325, pp.363-367.
- Gibbs, M.A. et al** (1991): 'Summary of the GULFEX flights, 23rd - 31st March 1991'. Met Research Flight, Royal Aerospace Establishment, Farnborough, England.
- Johnson, D.W. et al** (1991): 'Airborne observations of the physical and chemical characteristics of the Kuwait oil smoke plume', London: *Nature* Vol 353, No 6354, pp.617-621.
- Maryon, R.H.** (1992): 'The estimation of the optimal number of particles required for a regional multi-particle long range transport and dispersion model'. Proc 19th NATO/CCMS ITM on Air Pollution Modelling and its Application, Ierapetra, Crete, Sep/Oct 1991. [In press].

ANNEXES:

- Annex 1:** An account of the application of the Met Office meso-scale model to the Gulf plume, commencing 0000UCT 1st March 1991, with examples of the model output. (Mrs S P Ballard).
- Annex 2:** NAME output fields of trajectory end-points, concentrations of carbon in air, wet and dry deposition of carbon to the surface and time-integrated concentration (dosage) for the situation of Annex 1. The charts labelled A are without lofting of the plume due to the absorption of solar radiation; the charts labelled B include this effect.
- Annex 3:** Copies of the 1991 *Nature* articles by Browning et al and Johnson et al.
- Annex 4:** A copy of Maryon(1992).
- Annex 5:** Agreed proposals for the last phase of the work under contract, by H M ApSimon, Imperial College, London.

R.H.Maryon
Project Manager, NAME.
Met O(P), U.K. Met Office,
London Road, Bracknell, Berkshire, RG12 2SZ.
December, 1991.

ANNEX 1.

Mesoscale model simulations of smoke transport Notes on forecasts - ARATS project

S P Ballard and RTH Barnes
Short Range Forecasting Division, 8th August 1991

1. Introduction

Since 29th January 1991 30 hour mesoscale model forecasts for an area in the Gulf have been run routinely twice daily off special fine-mesh forecasts for that area (off global forecasts since 4th June). As the fine-mesh model grows its orography in the first 3 hours of the forecast it was sensible to start the mesoscale forecasts after the finemesh fields were in balance with the finer orography and forecasts are started at T+6. Forecasts are run with purely interpolated fine-mesh forecast data as the initial conditions (now global forecast data). For these forecasts smoke sources are included and the smoke is advected as a passive tracer (ie the interaction with radiation is neglected). For special investigations the model can be run including the interaction of radiation with the smoke.

2. Grid/model specifications.

The grid was originally centred on lat/long 29.5N 47.5E and uses a transverse Mercator projection with origin at centre and great circle running N-S along 47.5E.

Grid corners were NW 35.35N 40.23E NE 35.35N 54.77E
SW 23.30N 41.05E SE 23.30N 53.95E

No. of grid points were 89 W-E 91 N-S at 15km spacing,
i.e. grid covered 1320 x 1350 km.

There were 32 model levels (terrain following) at 1.25, 2.5, 5, 10, 20, 40, 70, 115, 175, 255, 355, 480, 630, 810, 1020, 1265, 1550, 1880, 2260, 2695, 3190, 3750, 4380, 5085, 5870, 6740, 7700, 8755, 9910, 11170, 12540, 14025m. Albedo = 0.25 increasing to 0.6 if snow covered .

From 25th February 1991 to 4th June the surface resistance to evaporation has been set to 500 sm-1 in the desert areas and 100 sm-1 over Iran and the Euphrates valley. Previously it was set to 100sm-1 everywhere. Since 4th June interpolated unified model values have been used outside the desert areas.

Also on 25th February it was decided to change the orography from the values interpolated from the fine-mesh. The new orography is interpolated from a U.S.Navy 10' resolution global orography dataset onto the mesoscale model grid. A simple interpolation gives maximum increase in height of 880m between 2 adjacent grid points on the western slope of the Iranian mountains and a max. height of 3077m, and this much steeper and higher orography caused one case with strong SWly winds to blow-up in the NE corner of the model. Therefore it was decided to interpolate in such a way as to give more detail over low ground (below 1000m) but a similar level of detail to the fine-mesh over the mountains of Iran. The new max. height is 2638 m and the max. increase between adjacent grid points 440m. All points with interpolated orographic heights less than 0m are set to -1m and assumed to be sea. This resolves the Gulf well without the need to modify by hand.

Roughness length is wind speed dependent over water. Since 25th February new values have been used over land. Previously the roughness length was

0.1m for heights greater than 500m and 0.001m elsewhere. The new values over land have been interpolated from 1.25°long x 0.833°lat data, prepared for the unified model, onto the mesoscale grid. Low roughness length values cover the desert SW half of the area with little dependence on orographic height while the low lying but cultivated Euphrates valley has higher values than before. The Iranian mountains have high roughness lengths as before.

On 19th April the area was moved northwards but dimensions kept the same. On 8th May the area was expanded to cover the original southern area as well as the north and the number of levels were reduced to 21.

The model formulation is as described in Golding 1990 (Met Mag 119 pg 81-96). Particular attention is drawn to the radiation schemes used in the model. A modified form of the longwave radiation scheme of Roach and Slingo(1979) is included. Heating rates are applied every timestep at every model level. The heating rates are derived from flux divergences which are recalculated every 15 minutes. The transmission functions are represented as products of functions for water vapour, carbon dioxide and cloud, the latter being weighted linearly by the maximum cloud fraction in the slab. The short-wave radiation budget is recalculated every time-step but only at two levels, the ground, and the highest cloud top if below 5km. At cloud top, absorption is parameterized as a function of solar zenith angle only, and is constrained not to exceed the long-wave cooling in the same layer. At the ground the transmission is obtained by applying, multiplicatively, transmission coefficients for Rayleigh scattering, water vapour absorption, aerosol scattering and cloud.

3. Inclusion of smoke plume.

The transport of the smoke is modelled by using the equation

$$\partial c / \partial t = -\mathbf{v} \cdot \nabla c + \partial (K_h \partial c / \partial \eta) / \partial \eta + K \nabla^2 c + S_c$$

where c is the aerosol concentration in kg/m/grid square

K_h is the vertical mixing coefficient for heat $\approx 1_h E_h$
 $\approx \text{fn}(1, E, N^2, S^2)$

$K = 22500 \text{ m}^2 \text{ s}^{-1}$

$S_c = \text{source in kg/m/grid square/s}$

all boundary conditions are $c=0$

$w'c'$ for the surface layer $= -c_h |v| c(1)$

$\partial w'c' / \partial \eta = 0$ at the top of the model

$c_{\min} = 5 \times 10^{-7} \text{ kg/m/grid square}$ is lower limit on concentration to remove any negative values generated by the finite difference scheme.

Since 18th April the concentrations have been in kg/kg so that the transport is conservative. However there is little difference in the results.

4. Source of smoke plume.

In the routine forecasts sources of smoke were originally added at locations identified from previous satellite imagery. Depths of sources are

also estimated from the imagery and the preliminary conclusions of the Gulf Task Group. The latter estimated an initial plume rise of 1-3km based on typical winter (January/February) conditions. This is consistent with reports from the Gulf and the evidence from satellite imagery that the majority of the visible smoke is remaining within the boundary layer. Therefore for most runs the source has been kept below 3km. Runs with injection up to 5km appeared to transport too much smoke with the upper level winds. Since 25th February a depth of 2260m has been used and the forecast smoke locations have generally agreed well with the imagery considering the limitations of the method of specifying the depths and locations of the sources. It is even harder to specify the total and relative strengths of the sources. This is why the routine forecasts are run neglecting the interaction with radiation. However the strengths have been estimated based on the imagery and using an upper limit of 5 Megatonne/year from all sources. The source is then distributed uniformly with height from the surface to source top over a single grid point.

From 25th February to 20th March the sources were kept constant as 3 point sources

location	depth	strength
30.5N 47.8E	2260m	5/38 x 5Mtonne/year
29.3N 47.6E	2260m	15/38 x 5Mtonne/year
29.2N 47.2E	2260m	15/38 x 5Mtonne/year

Better locations could be defined using the locations of known oil fields. However the above sources provided good predictions and since the output was provided to various users the locations were not updated. Forecasts with more distributed sources provided very similar results. On 20th March the number of source points was increased to 15 covering the main oil fields, each point had 3/38 x 5Mtonne/year. This gives a total input of greater than 5Mtonne/year but oil fields in northern Kuwait were included and it was not certain whether they were included in the initial source estimate, also source estimates were being questioned.

Although forecasts are run routinely no attempt, except in some special runs, is made to pass smoke from forecast to forecast. Therefore it is not possible to compare the early stages of the forecast with satellite observations as the smoke starts from zero in each run.

The plume is assumed to be non-buoyant and smoke removal (eg by washout and dry deposition) is ignored apart from that implied by the boundary conditions and surface fluxes.

5. Inclusion of absorption of solar radiation by smoke

If the interaction of the smoke with radiation is to be studied the absorption of solar radiation by the smoke can be modelled as suggested by Slingo (personal communication) by using

$$S(z) = S_0 \cos(Z) \exp(-ku / \cos(Z))$$

where Z is the solar zenith angle.

$S_0 \cos(Z)$ Wm^{-2} is the incoming solar radiation at the top of the atmosphere

k = absorption coefficient = $10 m^2 g^{-1}$

n=32

$u = \sum_{n=n(z)} C(n) \Delta z$

n=n(z)

$C(n)$ = concentration at level n in gm^{-3} = $c(n) \times 1000 / (15 \times 15 \times 10^6)$

The heating rate is then calculated as

$$\partial \theta_1 / \partial t = (g / c_p \pi) \partial S / \partial F$$

The solar fluxes and pressures are then calculated at midlevels.

In the implementation of the scheme the absorption due to smoke is used to reduce the solar fluxes reaching cloud top and the surface. However, in order to simplify the inclusion of the effects of smoke, the solar fluxes used in the calculation of heating rates due to smoke absorption are not reduced by the effects of clouds, water vapour, scattering and background aerosol. This means that there is a mismatch between the surface and atmospheric heating rates but the smoke absorption is a worst case scenario

6. Heat of combustion

This is not included.

7. Forecast for 02 3/3/91

Charts are attached from the 30 hour forecast from 18Z 1/3/91 valid at 02 3/3/91. These are from the routine forecasts with passive smoke - ie no interaction with solar radiation. This forecast has not been studied in detail and the output is just that produced routinely.

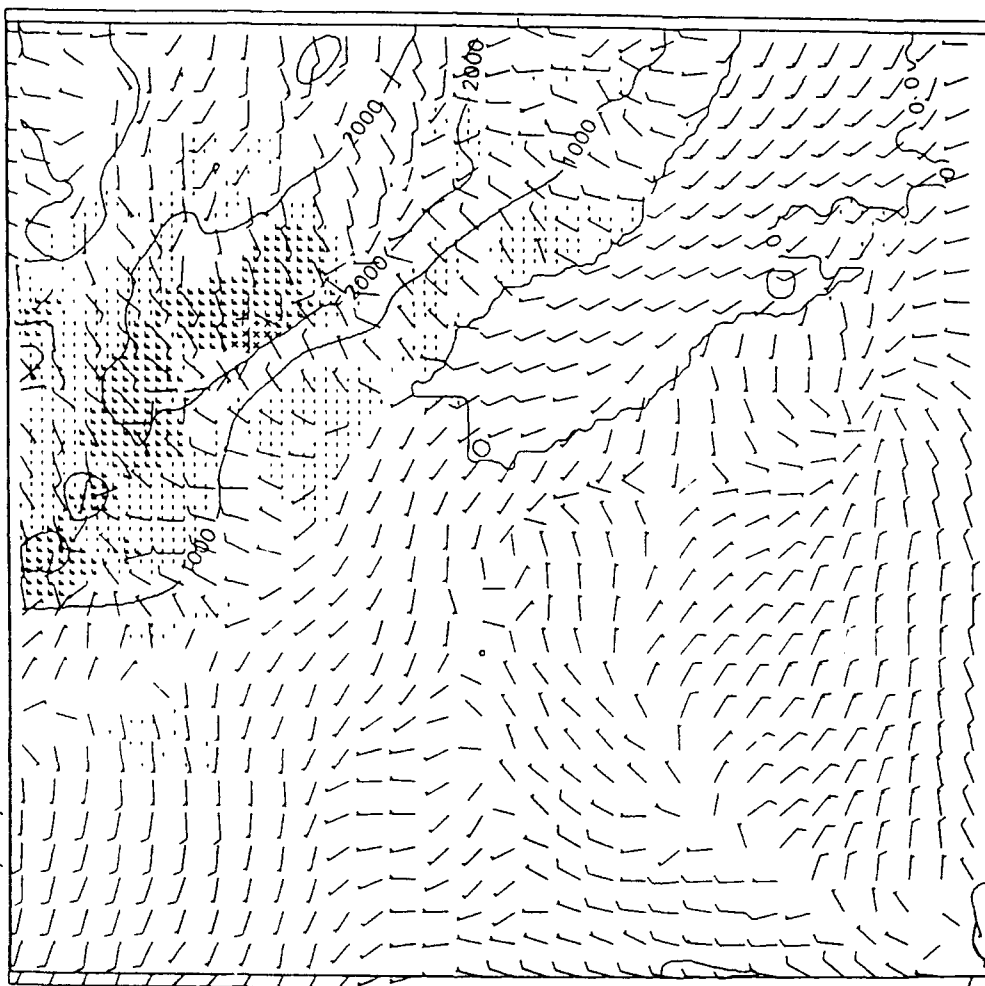
Chart A shows 10m wind and present weather with orographic height contours every 1000m. f = visibility less than 1km, - = visibility 1-5km. The visibility does not include the effects of smoke only cloud water, humidity and a default background value of aerosol suitable for the UK (ie not adjusted for desert areas etc)

Chart B shows 1550m wind and the vertically integrated column smoke density in kg/grid square. Horizontal lines are a problem with the contour routine.

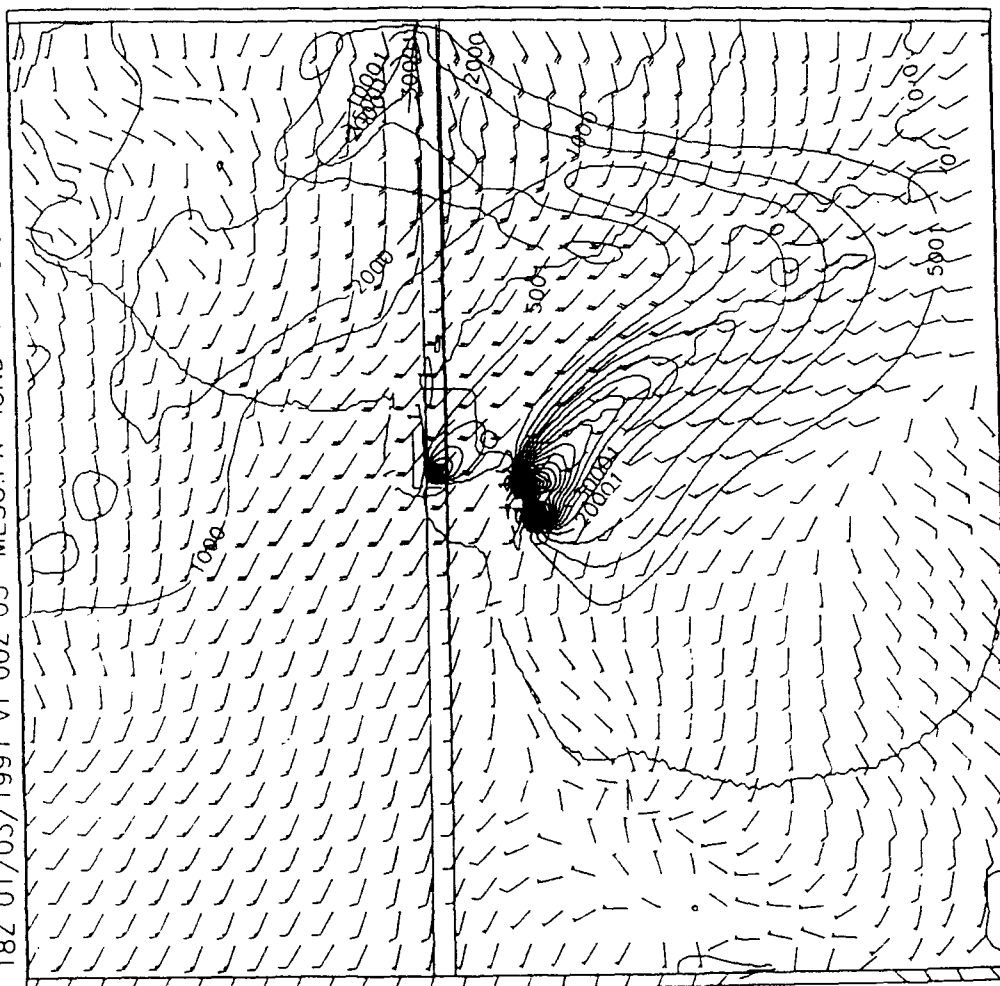
Chart C shows 480m wind and the smoke concentration at 480m in kg/grid square/m. Horizontal lines are a problem with the contour routine.

Chart D shows 1020m wind and the smoke concentration at 1020m in kg/grid square/m. Horizontal lines are a problem with the contour routine.

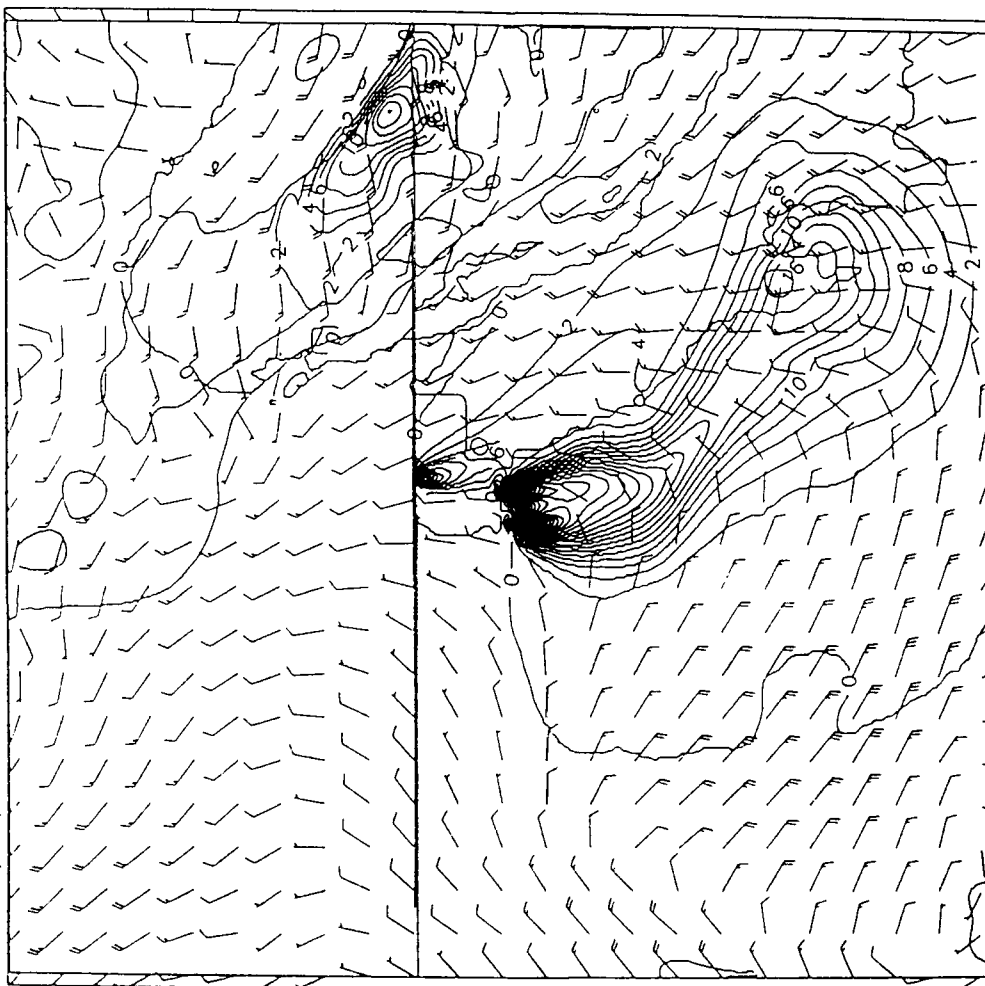
A DT 18Z 01/03/1991 VT 00Z 03 MESO.PR V AT 10.00M AG
DT 18Z 01/03/1991 VT 00Z 03 MESO.PR PRESENT WEATHER



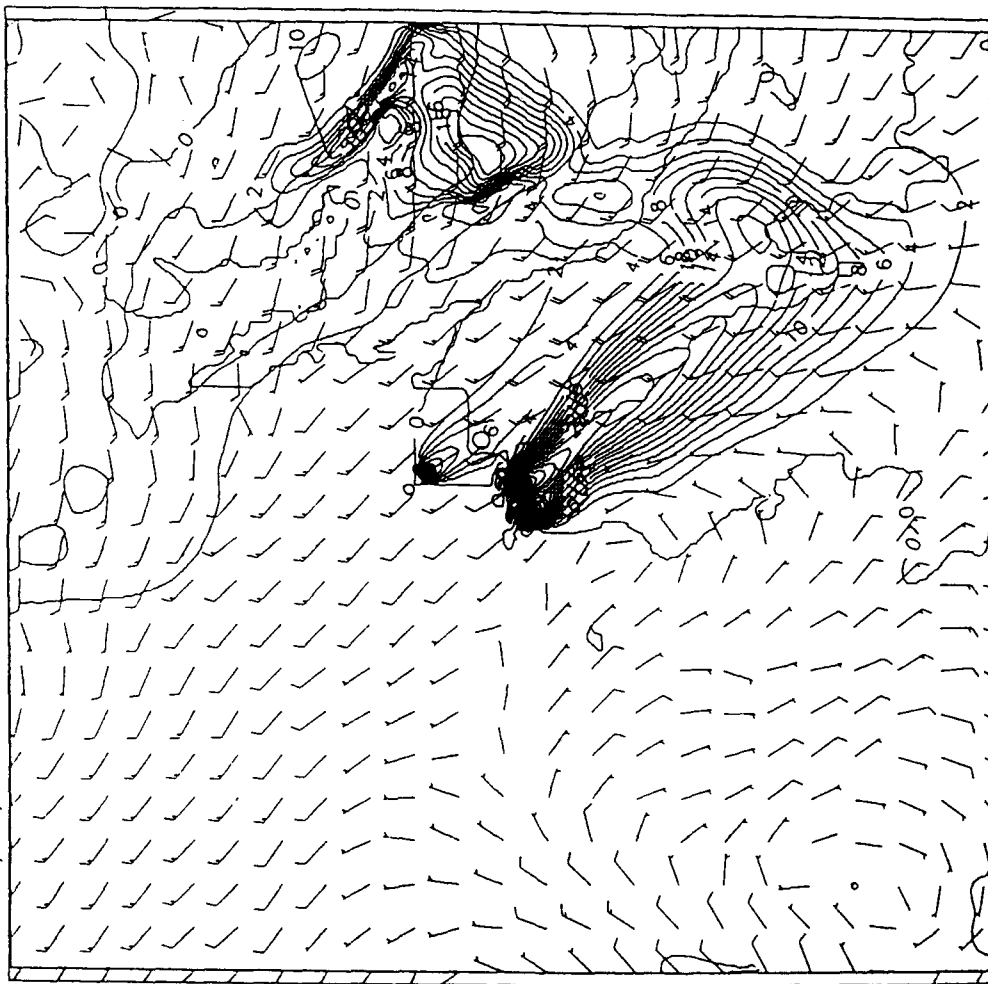
۷



C- DT 18Z 01/03/1991 VI 00Z 03 MESOPR U AT 480M AG
DT 18Z 01/03/1991 VI 00Z 03 MESOPR CNJD AT 480M AG

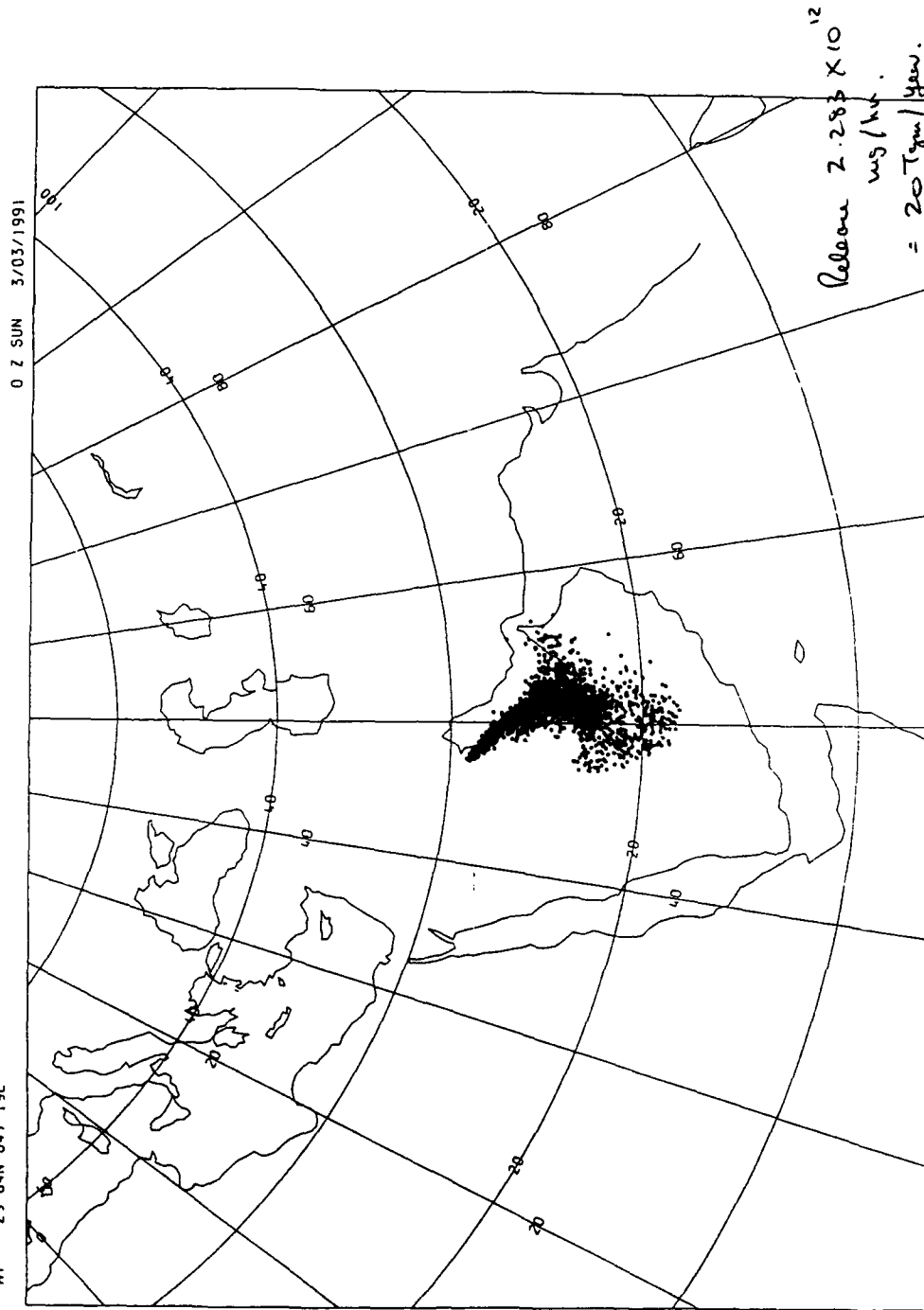


DT 18Z 01/03/1991 VT 00Z 03 MESO.PR V AT 1020M AG
DT 18Z 01/03/1991 VT 00Z 03 MESO.PR CN3D AT 1020M AG



METEOROLOGICAL OFFICE
FORECAST TRAJECTORY END POINTS IN BOUNDARY LAYER

RELEASE FROM 0000GHT 01/03/1991 - CONTINUING
AT 29 04N 047 19E

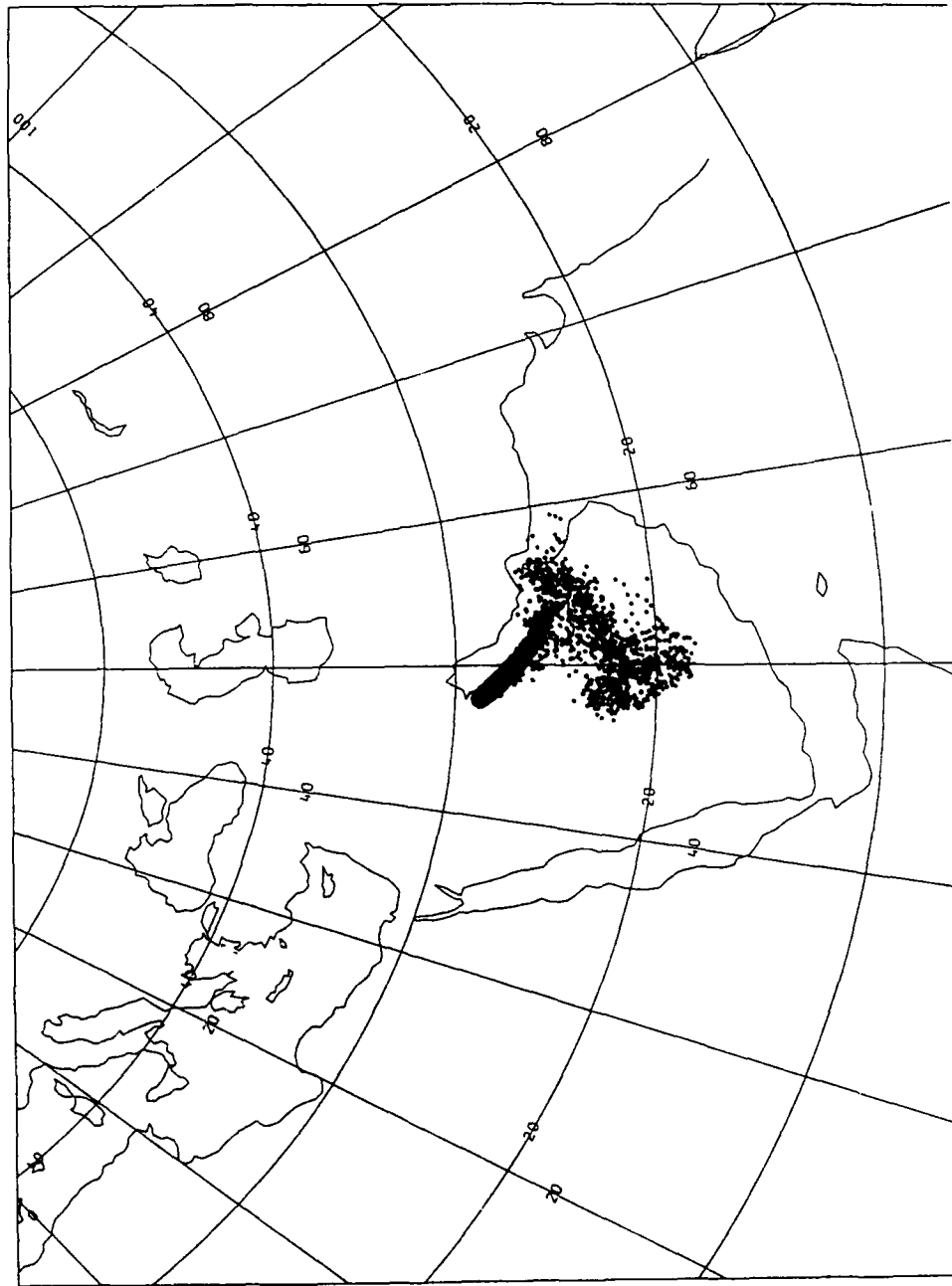


Annex 2.

METEOLOGICAL OFFICE
FORECAST TRAJECTORY END POINTS IN LAYER 3

RELEASE FROM 0000GMT 01/03/1991 - CONTINUING
AT 29 04N 047 19E

0 Z SUN 3/03/1991



METEOROLOGICAL OFFICE

FORECAST AIR CONCENTRATION (MG/M³) OF CARBON IN BOUNDARY LAYER $\times 10^2$

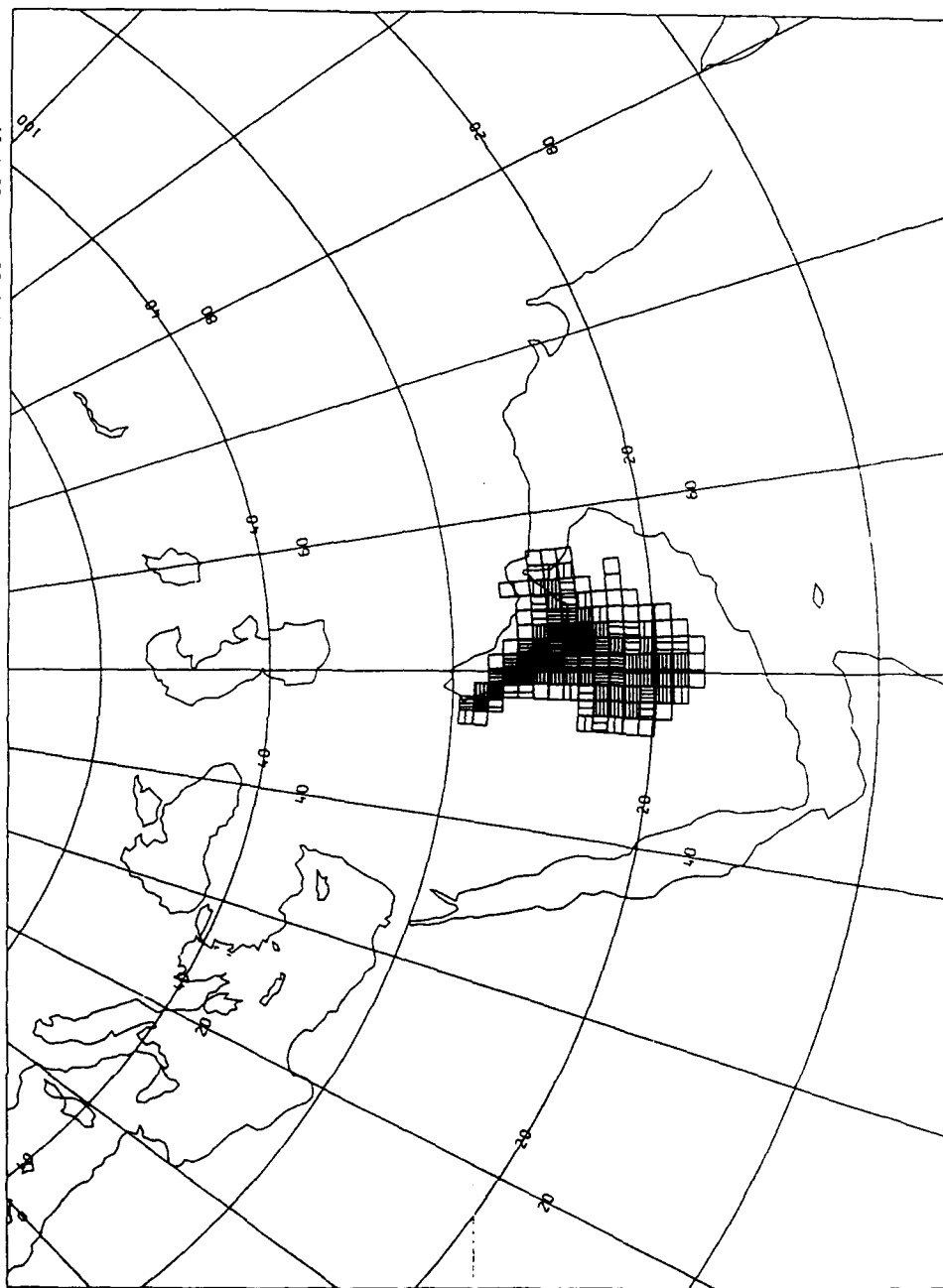
>0 - 1.83
 1.83 - 3.94

3.94 - 8.49
 8.49 - 18.29

18.29 - 39.41
 39.41 - 84.90



RELEASE FROM 0000GMT 01/03/1991 - CONTINUING
AT 29 04N 047 19E

0 Z SUN 3/03/1991





METEOROLOGICAL OFFICE

FORECAST AIR CONCENTRATION (HC/M=3) OF CARBON IN LAYER 3 X 10²

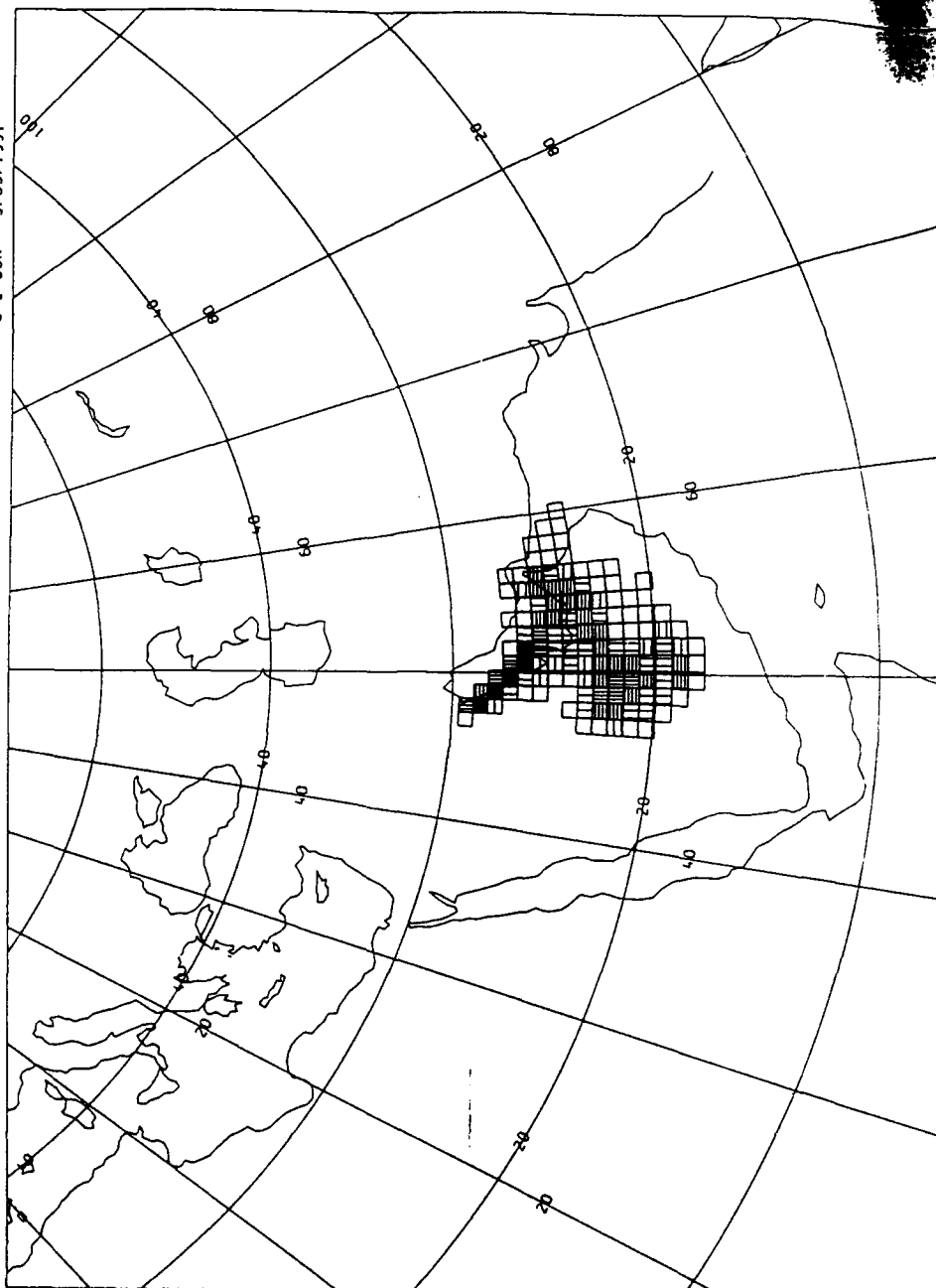
 >0 - 1.11
 1.11 - 2.39

 2.39 - 5.15
 5.15 - 11.09

 11.09 - 23.89
 23.89 - 51.47

RELEASE FROM 0000GMT 01/03/1991 - CONTINUING
AT 29 04N 047 19E

0 Z SUN 3/03/1991



METEOROLOGICAL OFFICE

FORECAST ACCUMULATED DRY DEPOSITION (GRM/M**2) FOR ALL SPECIES X 10²

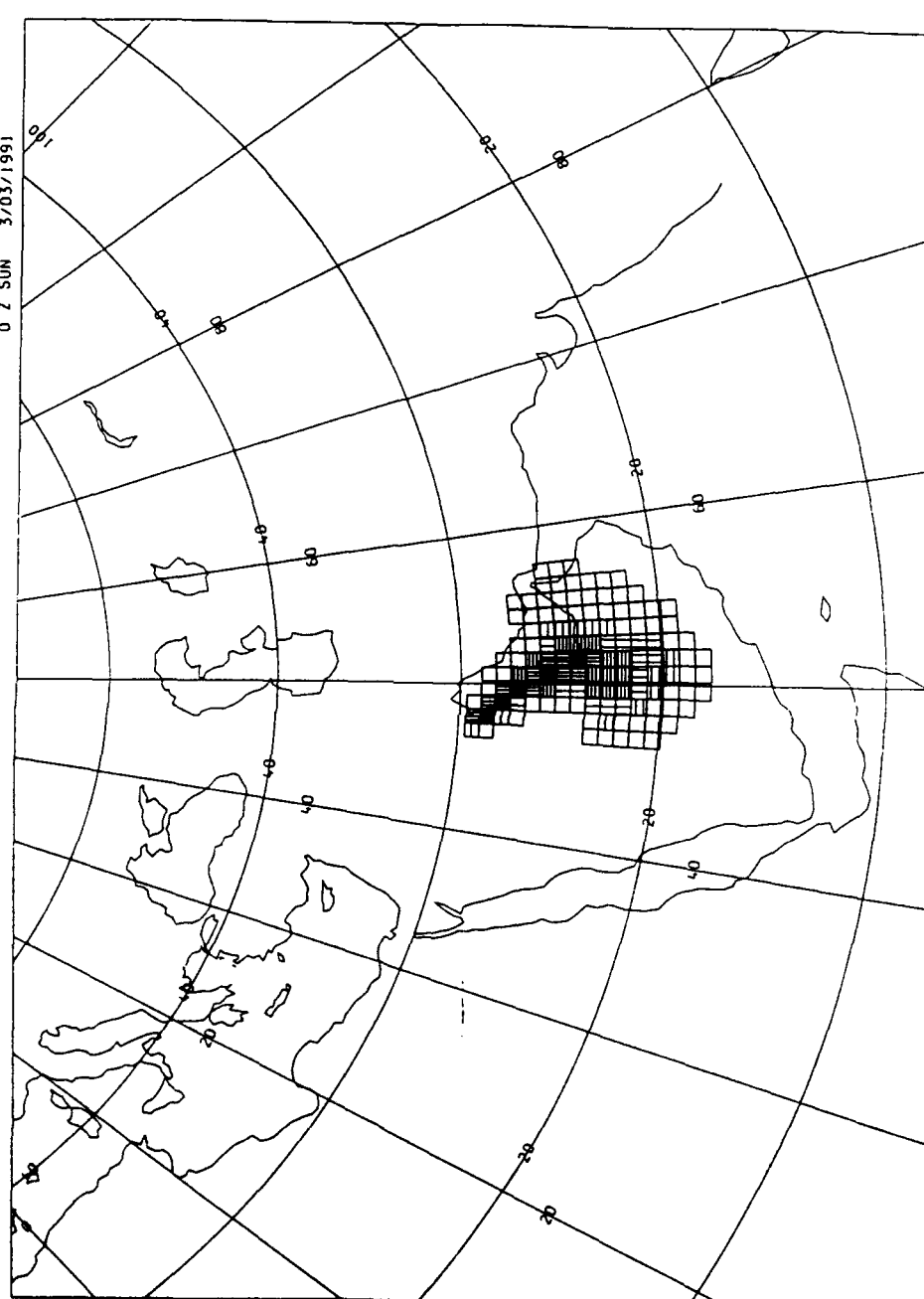
□ >0 - 0.10
 ▨ 0.10 - 0.22

▨ 0.22 - 0.48
 ▨ 0.48 - 1.03

▨ 1.03 - 2.22
 ▨ 2.22 - 4.76

RELEASE FROM 0000GMT 01/03/1991 - CONTINUING
 AT 29 04N 047 19E

0 Z SUN 3/03/1991



A

A

METEOROLOGICAL OFFICE

FORECAST ACCUMULATED WET DEPOSITION OF CARBON 110m-2 GRM / M=21



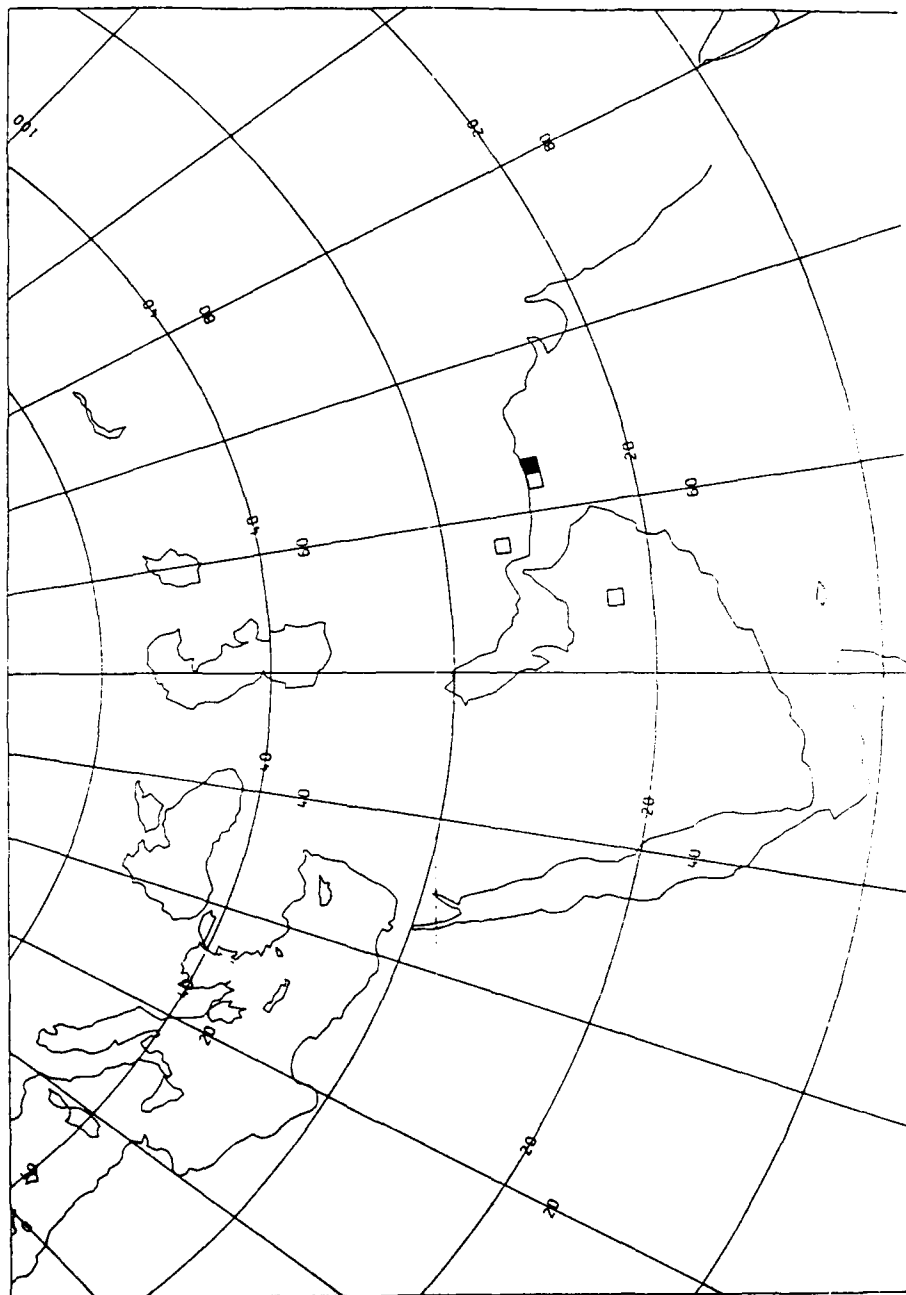
>0 - 0.01
0.01 - 0.01



0.01 - 0.01
0.01 - 0.01

RELEASE FROM 0000GMT 01/03/1991 - CONTINUING
AT 29 04N 047 19E

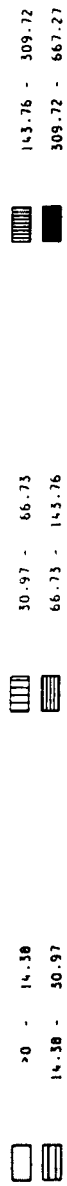
0 2 SUN 3/03/1991



A

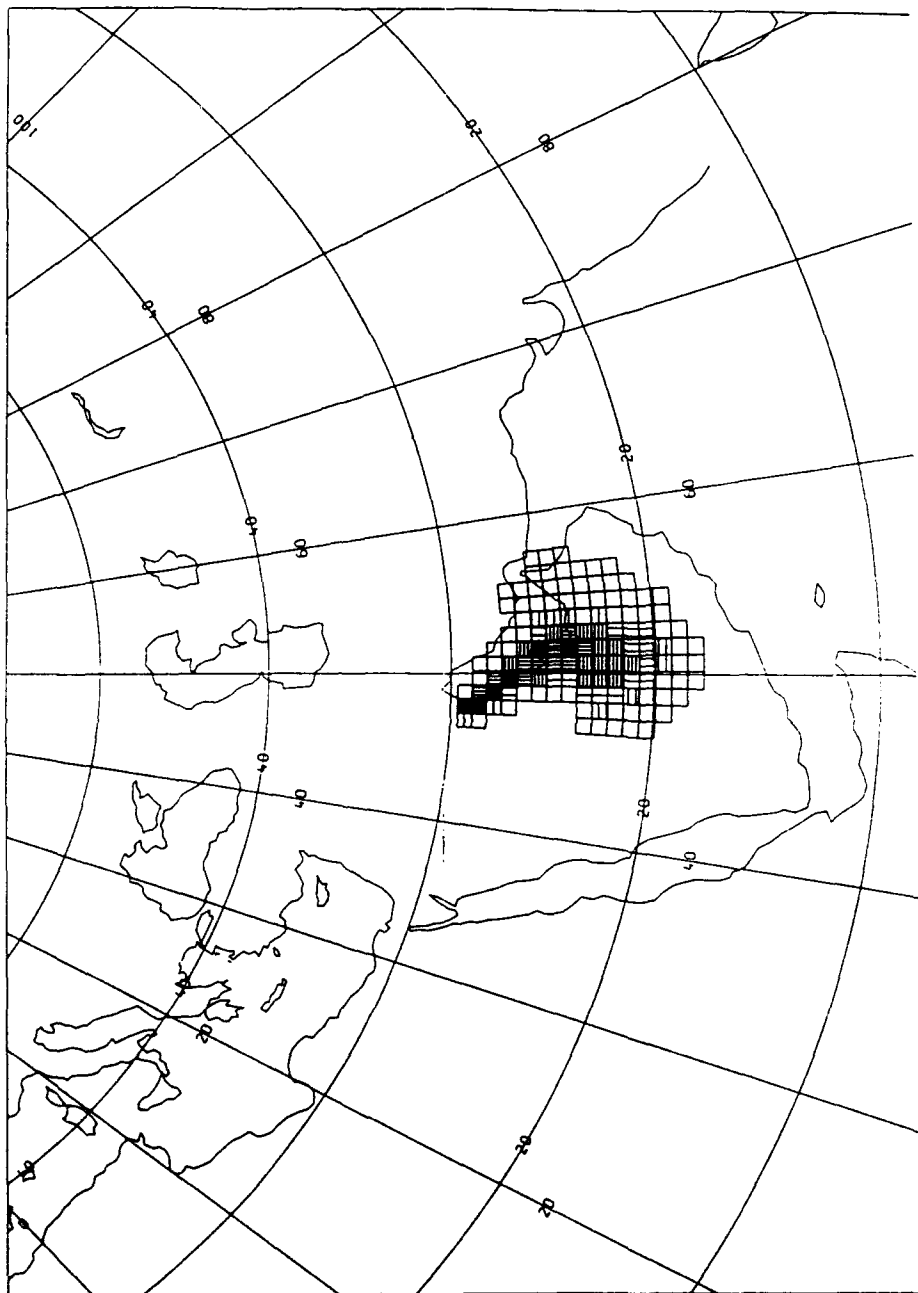
METEOROLOGICAL OFFICE

FORECAST DOSAGE (MCHM/M=3) INTEGRATED FOR ALL SPECIES IN BOUNDARY LAYER $\times 10^3$



RELEASE FROM 000000Z 01/03/1991 - CONTINUING
AT 29 04N 047 19E

0 Z SUN 3/03/1991



METEOROLOGICAL OFFICE

FORECAST ACCUMULATED TOTAL DEPOSITION (GRAM/H=2) FOR ALL SPECIES $\times 10^2$

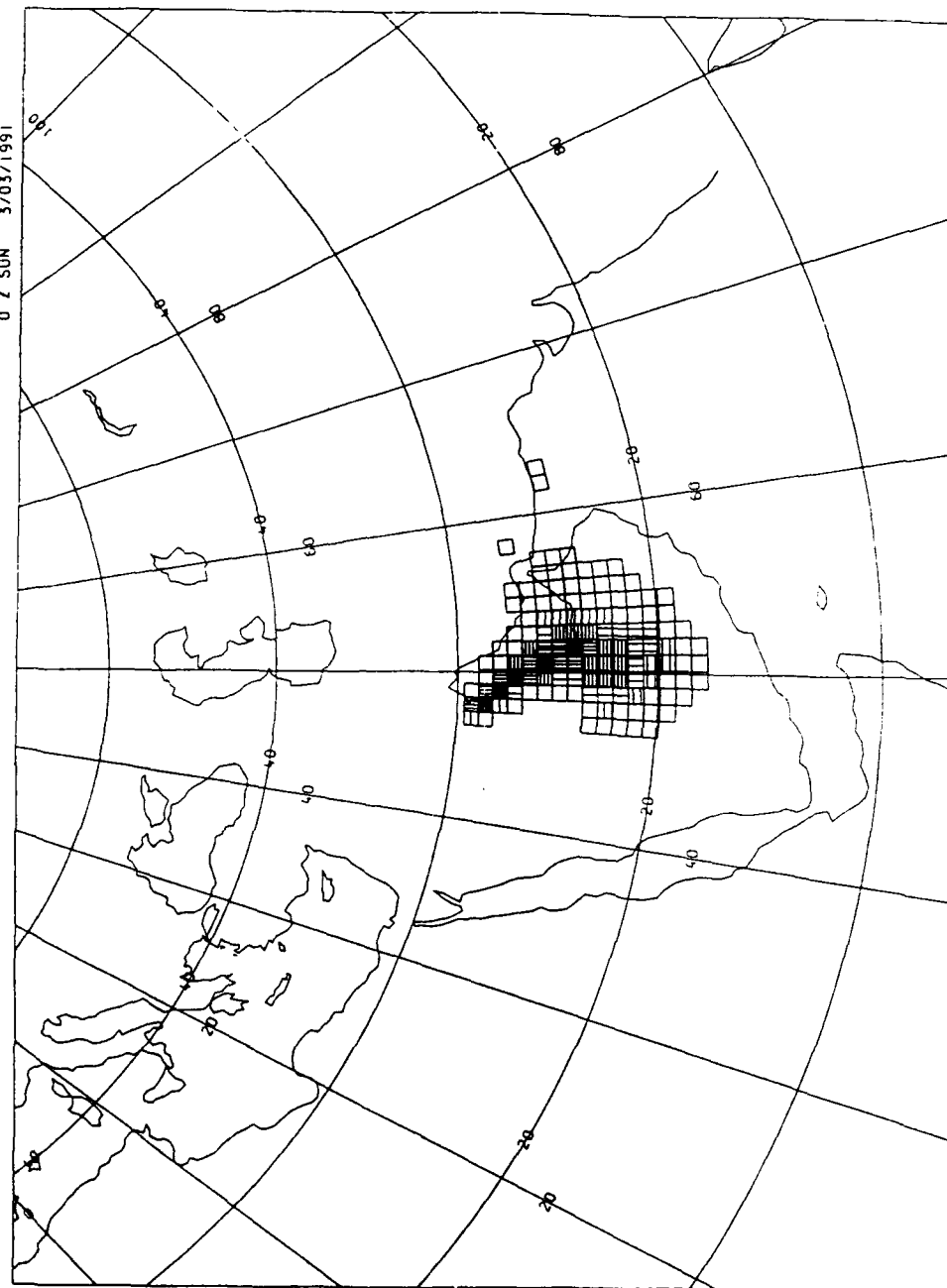
>0 - 0.10
 0.10 - 0.22

0.22 - 0.48
 0.48 - 1.03

1.03 - 2.22
 2.22 - 4.78

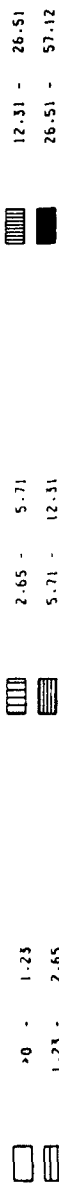
RELEASE FROM 0000GMT 01/03/1991 - CONTINUING
 AT 29 04N 047 19E

0 Z SUN 3/03/1991



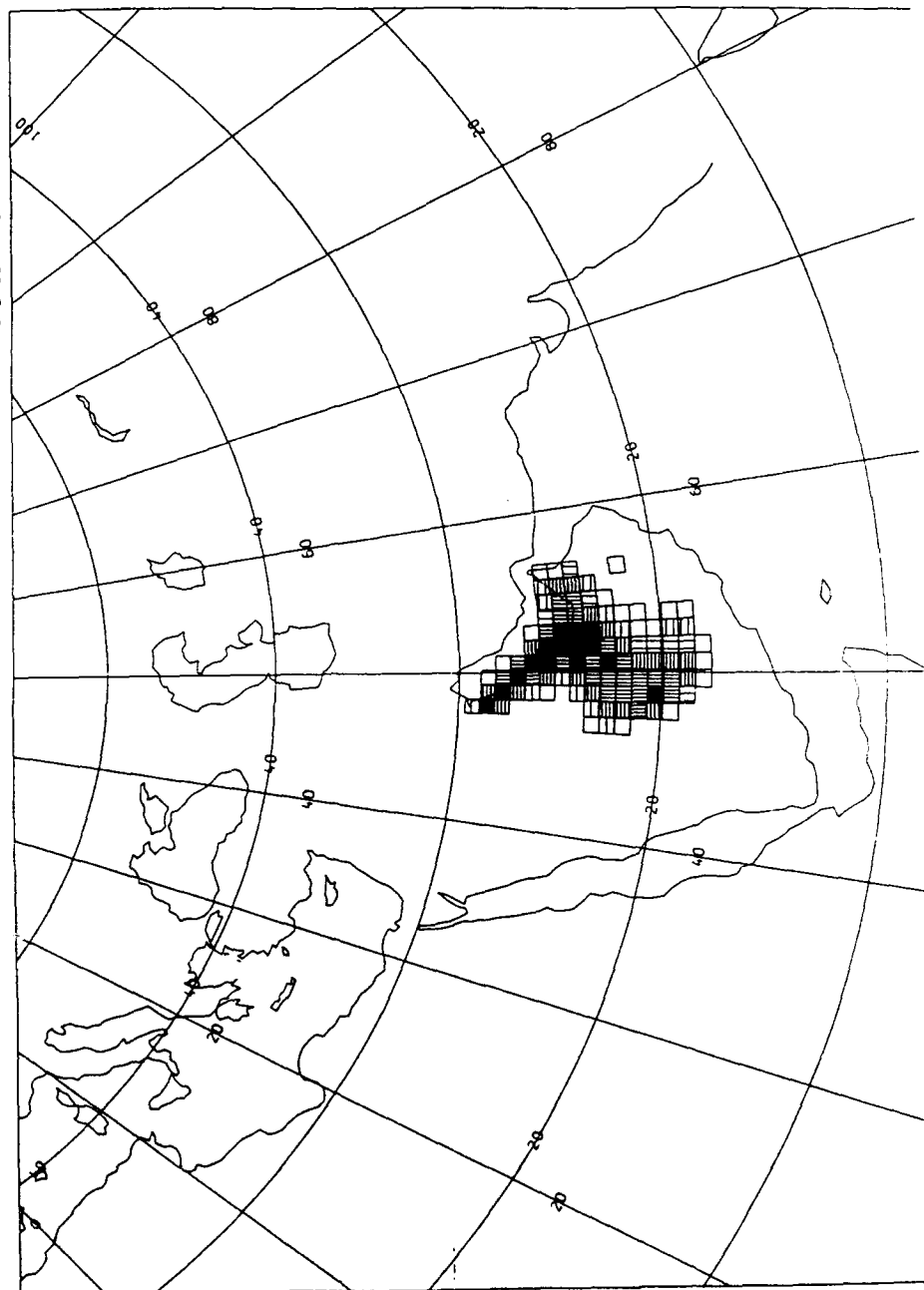
METEOROLOGICAL OFFICE

FORECAST AIR CONCENTRATION (MG/M³) OF CARBON IN BOUNDARY LAYER $\times 10^2$



RELEASE FROM 0000GMT 01/03/1991 - CONTINUING
AT 29 04N 047 19E

0 2 SUN 3/03/1991



METEOROLOGICAL OFFICE

FORECAST AIR CONCENTRATION (MG/M³) OF CARBON IN LAYER 3

X 10²

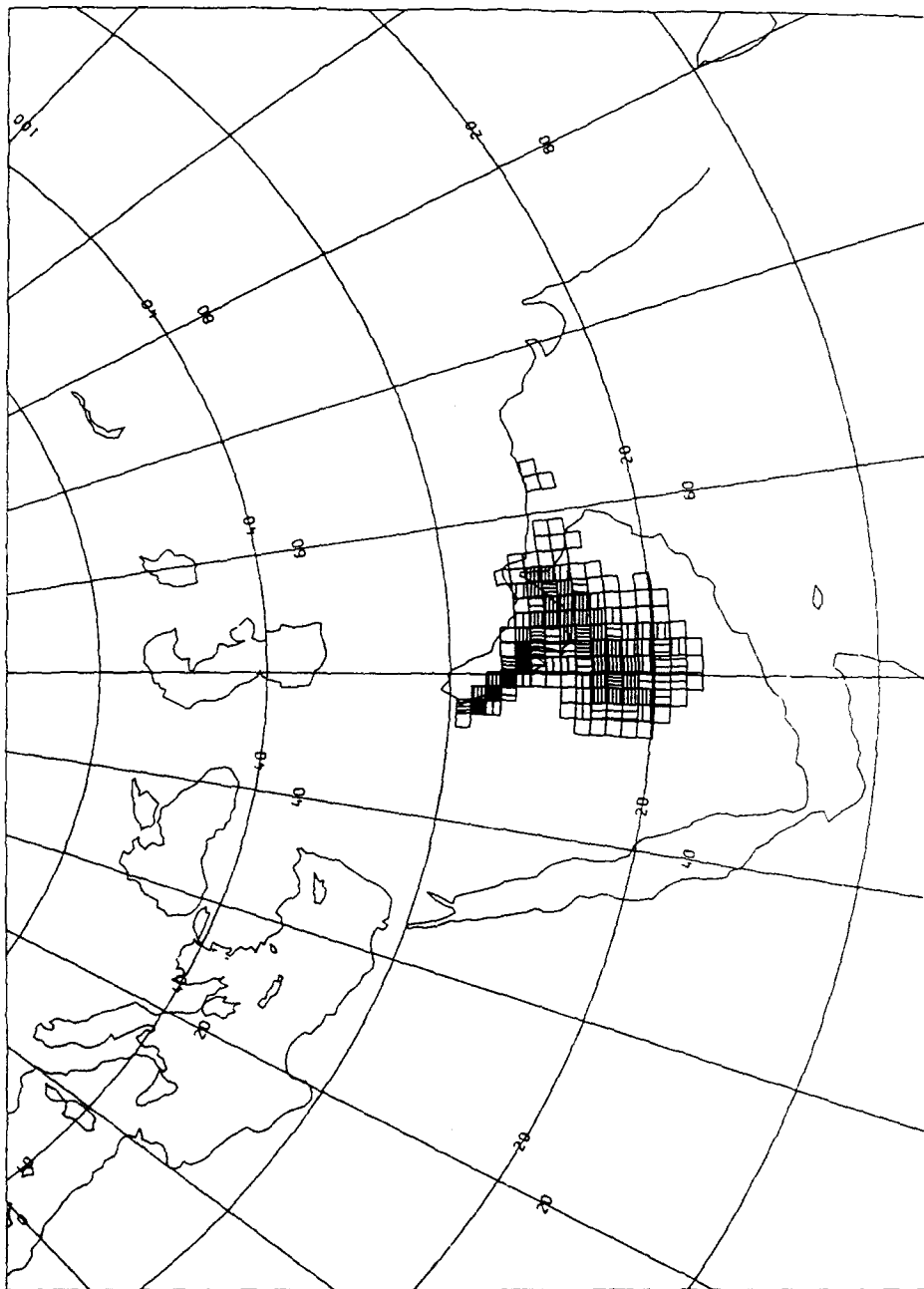
0 - 1.23
1.23 - 2.65

2.65 - 5.71
5.71 - 12.30

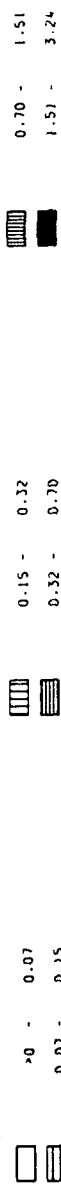
12.30 - 26.49
26.49 - 57.08

RELEASE FROM 0000GHT 01/03/1991 - CONTINUING
AT 29 04N 047 19E

0 2 SUN 3/03/1991

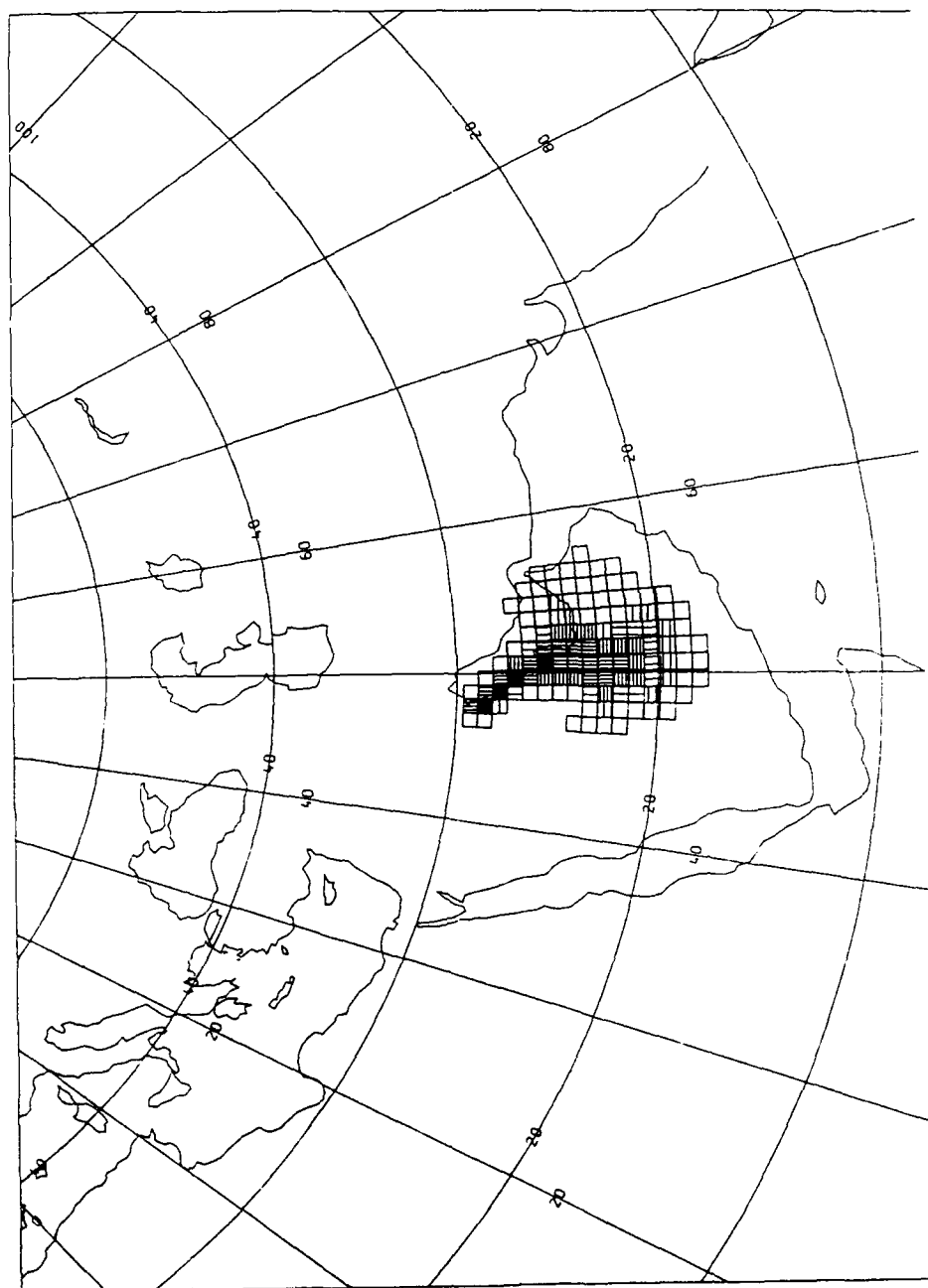


METEOROLOGICAL OFFICE
 FORECAST ACCUMULATED DRY DEPOSITION (G/M²/H) FOR ALL SPECIES



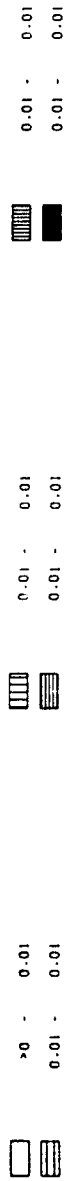
RELEASE FROM 0000GMT 01/03/1991 - CONTINUING
 AT 29 04N 047 19E

0 2 SUN 3/03/1991



METEOROLOGICAL OFFICE

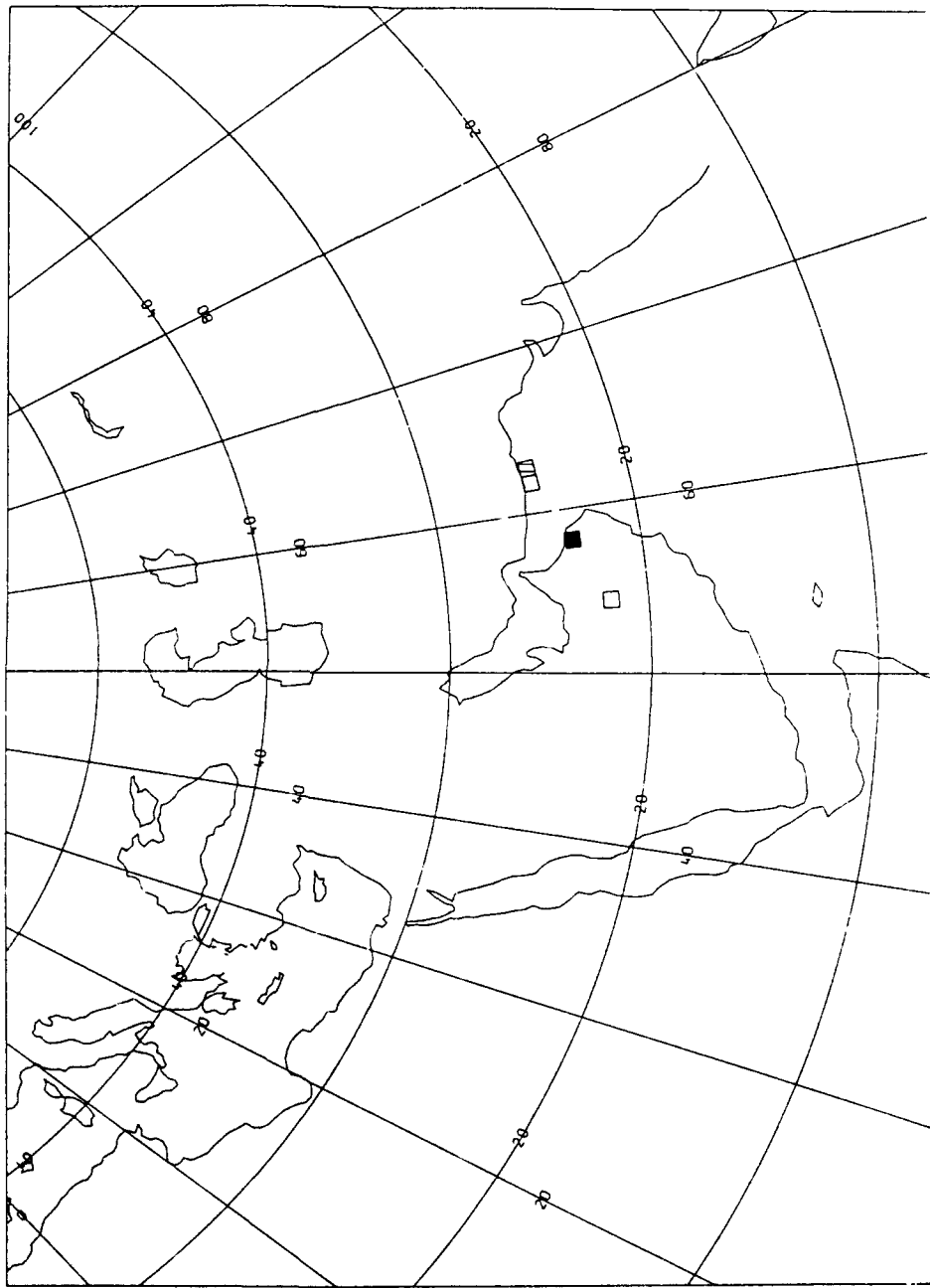
FORECAST ACCUMULATED WET DEPOSITION (GM/M²) FOR ALL SPECIES X (C)



RELEASE FROM 0000GMT 01/03/1991 - CONTINUING

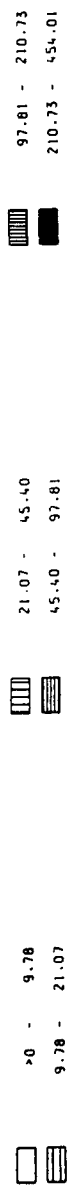
AT 29 04N 047 19E

0 Z SUN 3/03/1991

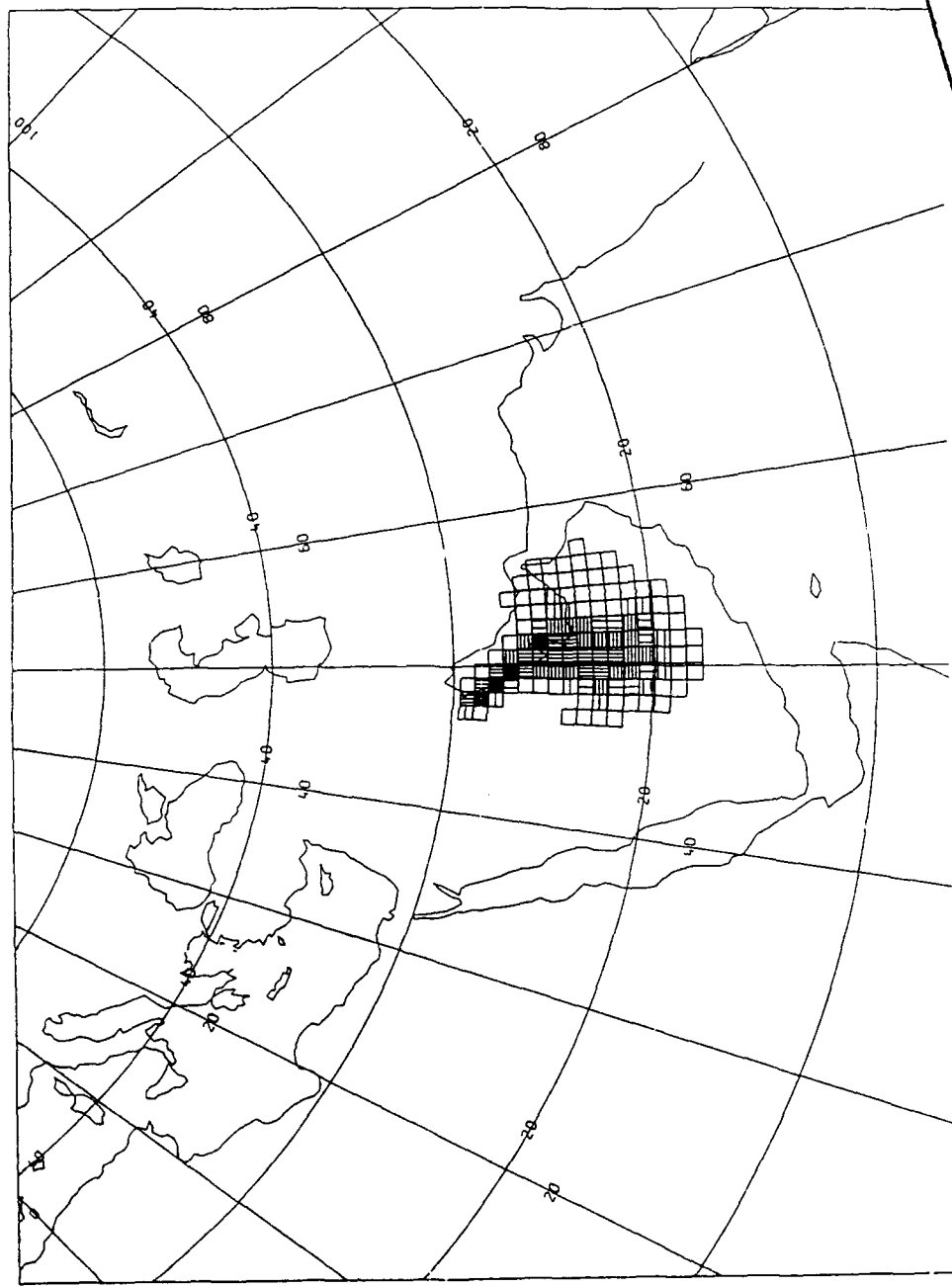


B

METEOROLOGICAL OFFICE
 FORECAST DOSAGE (MCHR/H=3) INTEGRATED FOR ALL SPECIES IN BOUNDARY LAYER X 10²



RELEASE FROM 0000GHT 01/03/1991 - CONTINUING
 AT 29 04N 047 19E



METEOROLOGICAL OFFICE

FORECAST ACCUMULATED TOTAL DEPOSITION (Gm/m²) FOR ALL SPECIES

X 10²

>0 - 0.07
0.07 - 0.15

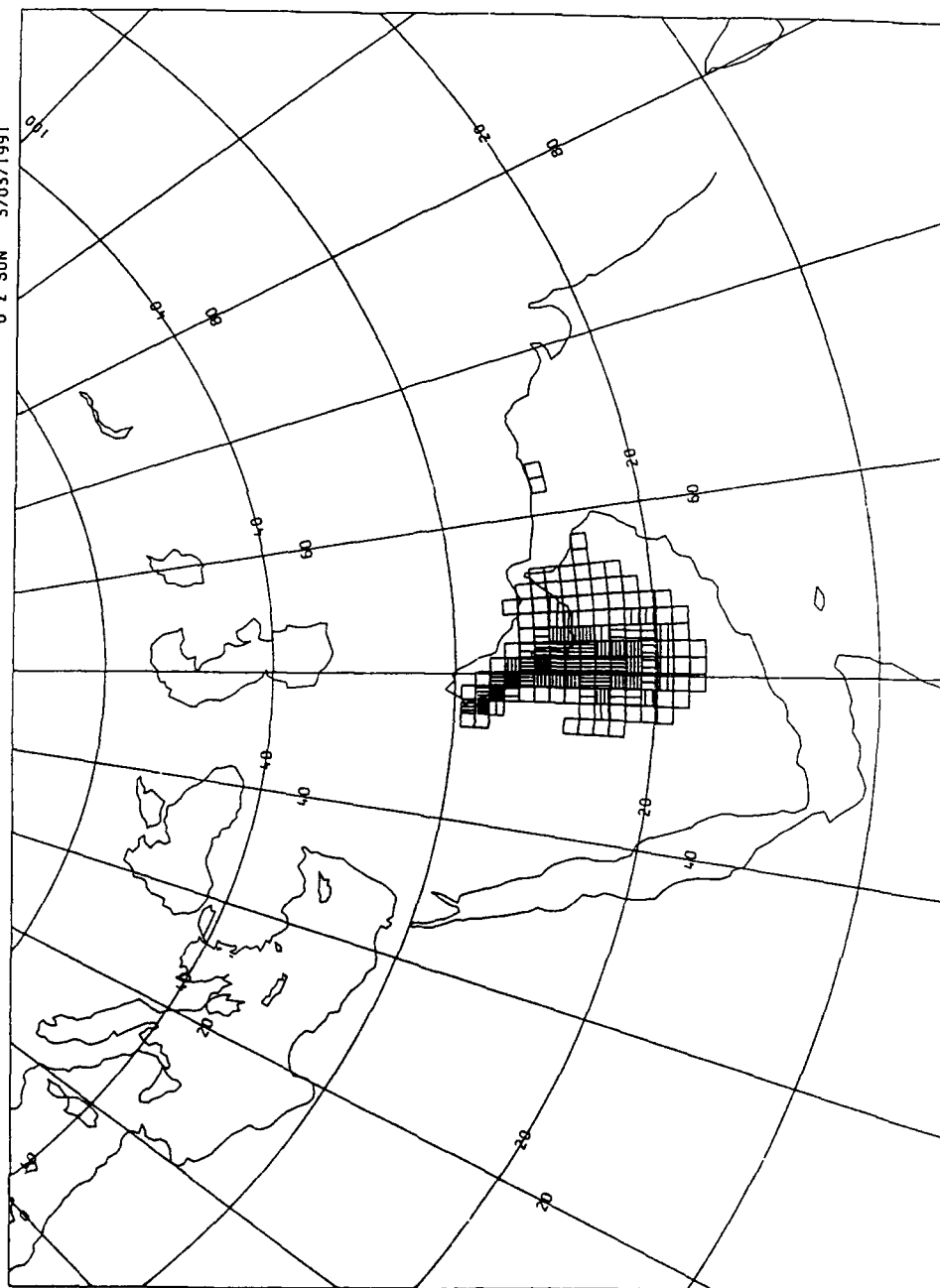
0.15 - 0.32
0.32 - 0.70

0.70 - 1.51
1.51 - 3.24

0.70 - 1.51
1.51 - 3.24

RELEASE FROM 0000GMT 01/03/1991 - CONTINUING
AT 29 04N 047 19E

0 Z SUN 3/03/1991



Environmental effects from burning oil wells in Kuwait

K. A. Browning, R. J. Allam, S. P. Ballard, R. T. H. Barnes, D. A. Bennetts,
R. H. Maryon, P. J. Mason, D. McKenna, J. F. B. Mitchell,
C. A. Senior, A. Slingo & F. B. Smith

Meteorological Office, London Road, Bracknell, Berkshire RG12 2SZ, UK

Model calculations, constrained by satellite observations, indicate that most of the smoke from the oil fires in Kuwait will remain in the lowest few kilometres of the troposphere. Beneath the plume there is a severe reduction in daylight, and a daytime temperature drop of $\sim 10^\circ\text{C}$ within ~ 200 km of the source. Episodic events of acid rain and photochemical smog will occur within $\sim 1,000$ – $2,000$ km of Kuwait. But changes in the Asian summer monsoon are unlikely to exceed the natural interannual variability and stratospheric ozone concentrations are unlikely to be affected.

THE main environmental effects arising from the burning oil wells in Kuwait come from emissions of oxides of carbon, sulphur and nitrogen, and unburnt hydrocarbons and particulates. The scenario used for this study¹, produced after discussion with the UK Department of Energy before the oil wells had been set alight, assumes 80 Tg of oil burning over a year, equivalent to the annual pre-invasion production of about 1.5 million barrels per day, with 6% of the oil being converted to fine particulate smoke. Small² assumed 1.6 million barrels per day, with 8.6% of the oil being converted to smoke. The products resulting from our scenario are given in Table 1, together with some current national and global emission figures for comparison.

We have used a simple model of plume rise to investigate the initial behaviour of the plume. We then used the Meteorological Office's mesoscale weather-prediction model to estimate the additional increase in height resulting from solar heating, the plume shape, and the daytime reduction in surface temperature, within a few hundred kilometres of Kuwait. For greater distances, out to several thousands of kilometres, we modelled the plume with the Meteorological Office's long-range dispersion model, which also provides estimates of wet and dry deposition. We also used data from a trajectory model as a basis for general circulation model integrations to determine the effect of the plume on the Asian summer monsoon.

Our study indicates that the smoke plume is very unlikely to reach the stratosphere, and the bulk of the smoke will remain within the lower troposphere before being deposited on the ground within a week or so of its emission. Consequently, changes in the Asian summer monsoon resulting from the smoke are likely to be small compared with the natural interannual variability. Beneath the plume within about 200 km of the source, it is likely that there will be a reduction in light to near night-time levels, and a reduction of the daytime maximum temperature of $\sim 10^\circ\text{C}$. The plume may remain visible for up to a few thousand kilometres, and slight reductions in daylight and temperature can be expected beneath it at distances of several hundred kilometres. Episodes of severe acid rain and 'black' snow, and photochemical smog, comparable with the highest

concentrations encountered around major industrial areas, are likely to occur out to distances of a thousand kilometres or more downwind. The carbon dioxide release (1% of current global emissions) will have an insignificant effect on global warming.

In general, we agree with Small² that effects will be significant in the Gulf region but insignificant on a global scale.

Local effects

During the first few minutes after emission, material in a smoke plume will rise rapidly, driven mainly by the heat from the burning oil. If we assume that the initial plume rise from each well is not enhanced by the effect of other wells, and use a heat source based on that expected from an average oil well (up to 500 MW), then simple calculations for turbulent plumes³ indicate that the smoke will reach an initial height of between 1 and 2 km in the range of stable conditions typical of winter. (Small² suggested a height of 700 m, but that was using a heat source of 319 MW.) In summer, when the well-mixed surface boundary layer deepens, smoke can be expected to rise to the top of the boundary layer, which can be 3 km deep (occasionally 4 to 5 km). In unstable situations, that is, in the presence of thunderstorms, the smoke could rise significantly higher, and some smoke might reach the upper troposphere; however, analysis of the Meteorological Office's climatological archives shows that these situations occur infrequently and are generally of short duration.

After the initial rise of the plumes they spread out and merge together. A further slow rise, termed 'self-lofting'⁴, may occur through solar heating. The consequence of this effect on the overall plume was investigated by using the Meteorological Office's mesoscale numerical weather-prediction model⁵, which has a grid scale of 15 km, adapted to include transport and diffusion of smoke in a manner similar to that developed for nuclear winter studies⁶. Transport of smoke by sub-grid scale convection, and removal by wet and dry deposition, were not included. In this and the other numerical models described later, incident solar radiation was assumed to be absorbed exponentially by the smoke with an absorption coefficient^{7,8} of $10\text{ m}^2\text{ g}^{-1}$. (Small² assumed $6.5\text{ m}^2\text{ g}^{-1}$ with a slightly greater amount of smoke.) The impacts of smoke on both scattering and infrared radiation were ignored. Nuclear winter studies⁷ show that neglecting the infrared properties of the smoke is a reasonable approximation when the particle sizes are predominantly less than one micrometre. The small infrared effects will act to ameliorate the predicted daytime surface temperature reduction and may reduce nocturnal surface cooling. The reduction of solar radiation by overlying cloud was also neglected, except at the surface, to simplify the model and to investigate the maximum possible impact.

Initial and boundary conditions for the mesoscale model were interpolated from the UK Meteorological Office's operational regional model forecasts. Throughout the period of the forecast, smoke was injected uniformly from the surface to a specified plume top. Forecasts were run for five selected days in January, February and March 1991 with and (as a control) without the interactive effects of absorption of solar radiation by smoke. We

selected cases to cover the two main synoptic situations: cloudy cyclonic, when the smoke was advected to the north over Iraq and Iran, and clear anticyclonic, when the smoke was advected to the southeast over Saudi Arabia and the Gulf. For January and February, the smoke sources were distributed uniformly over a square of side 45 km, from the surface to a height of 4 km. For the later cases, point sources of smoke were inserted from the surface to 2.5 km, at locations identified from satellite images. The plume height was deduced by comparing the forecast vertical wind profile with the direction of transport of the bulk of the observed smoke.

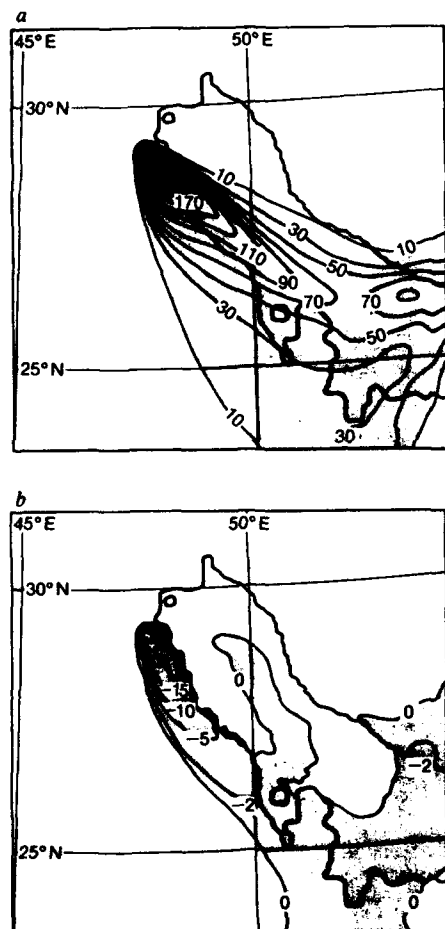


FIG. 1 Thirty-hour forecast of the Kuwaiti smoke plume valid at 12 GMT, 23 February 1991 (see also Fig. 2c), from the mesoscale model. a. Column-integrated distribution of smoke, S , in mg m^{-2} (optical depth $= S \times k \times 10^{-3}$, where the absorption coefficient $k = 10 \text{ m}^2 \text{ g}^{-1}$). b. Differences in screen-level (1.25 m) temperature due to absorption of solar radiation (contours at intervals of -5°C with contour added at -2°C). The smoke source, centred at 29.1°N , 47.8°E , is 5 megatons per year spread over a square of side 45 km, with its top at 4 km. The model domain is 1,350 by 1,320 km in the horizontal by 14 km in the vertical with a horizontal grid resolution of 15 km and 32 levels spaced irregularly in the vertical.

TABLE 1 Assumed annual production of the Kuwaiti fires

Type of emission	Amount (Tg per yr)	Comparison with current emission
Fine particulate black smoke*	5	Roughly a third of the carbon particles produced through tropical biomass burning ²²
Sulphur (as sulphur oxides)	2	Slightly more than the current UK annual sulphur emissions ²³
Nitrogen (as nitrogen oxides)	0.5	1988 UK nitrogen oxide emissions ²³ were 0.75 Tg
Carbon (ultimately as carbon dioxide)	60	About 1% of current global annual carbon dioxide emissions from fossil fuel combustion

* Small² assumes 5.8 Tg of smoke per year.

† Small (personal communication) suggests 3.3%.

The figures are compared with current national and global figures. The percentage of sulphur in Kuwaiti oil varies from field to field, but an average value is 2.5%† (figure provided by the Department of Energy). The percentage of nitrogen in the fuel is $\sim 0.17\%$ (Department of Energy), but to this must be added the quantity of nitrogen oxides produced during combustion (above $\sim 2,000 \text{ K}$); we have assumed an overall figure of 0.6%.

In the control runs, the smoke remained below the top of the initial source for four of the cases. In the fifth forecast, south-westerly flow over the Iranian mountains lifted significant quantities of smoke from 2.5 to 4 km, and trace amounts reached 8–12 km in regions of convection. Peak concentrations of smoke were forecast just above the top of the boundary layer in all forecasts irrespective of the initial height of the source.

When the effects of solar absorption were included, lofting of smoke in significant quantities was limited to a rise of 1–3 km above that in the control integrations. With flow down the Gulf, and solar absorption included, small amounts of smoke reached 8 km. It is not clear whether this was due solely to self-lofting or partly due to the effects of induced mesoscale circulations, possibly through changing land-sea boundary effects (the model, in agreement with satellite imagery, sometimes generated cloud in the regions where smoke was elevated).

The predicted rise of the smoke is low compared with the typical height of the tropopause (15 km) over Kuwait. Therefore, with the smoke failing to reach the stratosphere, its lifetime can be expected to be relatively short (see later), and close analogies with nuclear winter²⁻¹¹ and large volcanic eruptions¹¹ are inappropriate.

We also assessed the impact on surface temperatures of absorption of solar radiation. There is a large variability in the position of the plume, and the associated cooling and reduction in light levels, because of the day-to-day variability of the wind. Figure 1a shows the smoke distribution (compare also with Fig. 2 later), and Fig. 1b gives the associated reduction of surface temperature for 23 February 1991. The maximum daytime temperatures at screen level are depressed by about 10°C beneath the high concentrations of smoke within about 200 km of the source, and temperature drops of one or two degrees are predicted hundreds of kilometres downstream from the source. The drop of 20°C shown in Fig. 1b near the source region is likely to be excessive. The model cannot resolve the details of the flow on that scale, and the smoke concentrations may be large enough that infrared effects can no longer be ignored. Results will also be sensitive to the assumed surface characteristics and the modelling of the surface layer mixing. Sunlight is reduced to near night-time levels in the model when thick smoke is overhead, but the model cannot represent sub-grid-scale structure, and this may allow a little sunlight to penetrate.

From mid-March to mid-April, we have compared daily operational forecasts of midday temperatures in the absence of

the smoke with such observations as were available from stations beneath the plume (typically 4–8 observations per day when the plume extended south, very few when it extended north). Checks on the forecast values were provided by stations in unaffected regions. This subjective assessment suggests that within ~250 km of the source the reductions in midday temperature under the plume ranged from 5 to 8 °C, decreasing to 1–2 °C (probably the limit of accuracy) beyond about 750 km.

Effects at longer range

The Meteorological Office's long-range dispersion model¹² was used to investigate the longer-term distribution of the smoke, and also the acid rain and photochemical smog that may occur before concentrations reach more normal background levels.

The model simulates the spread of neutrally buoyant airborne pollutants (for example fine soot or sulphur) by releasing very large numbers of 'particles' into the model's atmosphere at the source of the pollution. The particles are transported by the model winds and vertical motions, and are diffused vertically and horizontally by random perturbations, which represent the small-scale turbulent motions likely to be experienced in the real atmosphere (especially near the surface). The model has been run daily since February to monitor the concentration of the smoke particles for a number of levels in the vertical. These integrations neglected self-lofting.

Six integrations were re-run with solar absorption included, as in the mesoscale model, and the particles allowed to self-loft in parcels to the level of neutral buoyancy. Comparisons between the integrations with and without solar absorption showed that in strong sunlight a small proportion (typically 5%) of the model's particles lofted rapidly through a kilometre or more. Thinning of the plume by entrainment, coupled with the model's normal turbulent diffusion, reduced the lofting to the point at which other vertical motions dominated, usually within one or two days. For an injection height of 2 km, the amount of smoke reaching 3–5 km was slightly augmented, but most of the material (90%) remained at lower levels.

Close to the source, results were similar to the mesoscale model. An example of the shape of the smoke plume at different heights is shown in Fig. 2a and b. In the boundary layer, below 1.5 km, the plume extends southwards and fans out; between 1.5 and 3 km, it encounters winds with a westerly component, and it drifts eastwards across the Gulf. Pictures from the geostationary satellite Meteosat, monitored with a dedicated computer display system, broadly confirmed the model forecasts. The visible image for the time corresponding to Fig. 2a and b shows the plume rapidly broadening towards the south as it

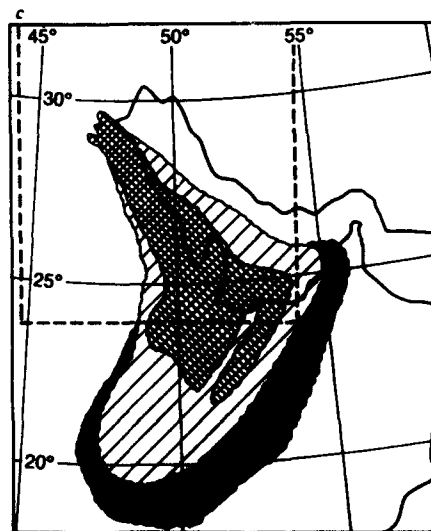
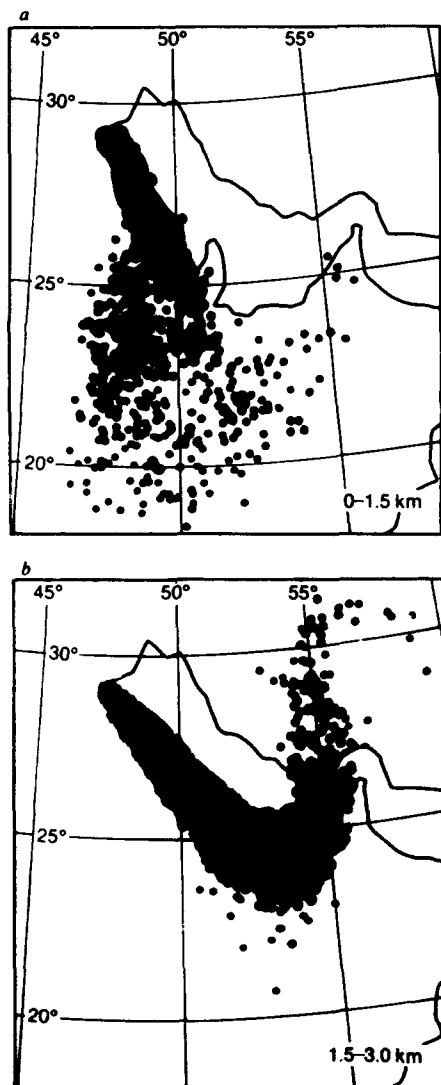


FIG. 2 Forty-eight-hour forecast, valid at 12 GMT, 23 February 1991, from the long-range dispersion model. a Shape of the Kuwaiti smoke plume over the height interval 0 to 1.5 km; b 1.5 to 3 km, as derived from the long-range dispersion model assuming that the smoke extended from 0.5 to 4 km altitude at source. These may be compared with the analysis of the Meteosat visible image for the corresponding time (Fig. 2c), where cross-hatched, hatched and stippled shading represent subjectively determined regions of different optical thicknesses. The dashed frame in c shows the area in Fig. 1.

encounters flows at different levels, before thinning to such an extent as to be undetectable (Fig. 2c).

To estimate the lifetime of the smoke, the 'mass' (corresponding to a small proportion of the source emission) carried by each model particle was progressively reduced to take account of the estimated wet and dry deposition to the surface. A standard deposition velocity for dry particles (0.05 cm s^{-1} , valid over the boundary-layer depth) and scavenging coefficient in rain ($1.2 \times 10^{-4} \text{ s}^{-1} \text{ per mm h}^{-1}$) were assumed for the smoke^{13,14}. Initial and boundary conditions, and rainfall rates, were taken from the operational analyses and forecasts of the Meteorological Office's regional model. Fourteen cases were considered. The half-life of the material was typically 5–15 days, except in very wet conditions, when it was shorter, and in deep dry boundary layers, when it was longer. Small² estimated a half-life of 5 days and MacCracken¹⁰ computed 3.5–6 days, depending on the depth of the release.

Although dry deposition is the principal process for removing gaseous sulphur dioxide from the plume, it is less important for 'sulphur' aerosol or sulphur attached to particulates, and the time-integrated dry deposition at a given location is unlikely to cause significant ecological damage, except possibly within the immediate area of the fires where the droplets of unburnt oil fall out under gravity. Wet deposition, although contributing less to the overall depletion of sulphur, will often be associated with locally very acidic rain. Measurements of pH in eastern Saudi Arabia¹⁵ taken before the Gulf War had a mean of almost 5.5, and therefore the associated background ions are unlikely to reduce the acidity generated by the plume significantly. We made calculations assuming plume widths (typically ~200 km) and depths (3–4 km) based on our model results and satellite observations. Allowing for saturation in the uptake of acidic species into growing raindrops, the results indicate that, once rain is encountered, its acidity will depend only weakly on downwind distance out to at least 2,000 km, with pH values in the range 3.0–3.6 on many occasions. These very acidic values could damage crops and vegetation¹⁶.

Over the higher mountains much of the precipitation falls as snow and, where it is affected by the emissions, the snow may be blackened enough by soot to darken it considerably. Forecasts from the mesoscale model (such as in Fig. 1a) occasionally show average smoke-column densities of ~40 mg m^{-2} over the southern Iranian mountains. If this were scavenged by snowfall with a water equivalent depth of 1 mm, the mass mixing ratio

of soot within the snow would be typically 10^{-5} , which could double the absorption of solar radiation⁴. Spring snow-melt could therefore occur earlier and faster, with the possible consequence of high run-off and highly acidic pulses in the rivers.

Close to the source of the plume, the low light levels are expected to prevent any significant photochemical effects, except at the top of the plume. As the plume disperses, however, light levels will recover to values more typical of the region. This will allow rapid oxidation of hydrocarbons and other gases (such as H_2S) within the plume, probably over a timescale of a few days, resulting in locally severe episodes of photochemical smog.

Effect on the monsoon

To determine whether the smoke emissions are likely to affect the Asian monsoon, we carried out an idealized sensitivity experiment with a version of the Meteorological Office's atmospheric general circulation model that has been used extensively for seasonal predictions of tropical rainfall¹⁷; this version was chosen because it produces a good simulation of the Asian monsoon. The radiative effects of the smoke were included as in nuclear winter studies¹⁸; this approach was similar to the simple formulation in the mesoscale model described above, except that we included the effect of shading by clouds on the radiative heating of the smoke.

The distribution of smoke used in this model was derived from the wind fields actually observed in two previous years, 1989 and 1990, using the global trajectory facility attached to the numerical weather-prediction model of the European Centre for Medium-Range Weather Forecasting¹⁹. A smoke particle was released once a month from each of the vertices of an area of $1^\circ \times 1.5^\circ$ covering Kuwait at each of the four levels 950, 850, 700 and 500 mbar, and their three-dimensional trajectories were followed during an assumed 10-day lifetime. Figure 3a and b shows the resulting density of smoke at two different levels, averaged over the period of the monsoon, April to September.

For the sensitivity experiment, we prescribed purely absorbing smoke (absorption coefficient $10 \text{ m}^2 \text{ g}^{-1}$), with a smoke loading of 0.012 g m^{-2} (vertical optical depth 0.12) centred on Kuwait and mixed evenly throughout the troposphere up to a height of 8 km. The distribution of the smoke in Fig. 3 was approximated by $a^2/(a^2 + r^2)$, where r is the distance from source, and a was set at two model grid lengths (~600 km). The total smoke loading is equivalent to assuming a smoke lifetime of 10 days with emissions at a rate of 5 Tg per year.

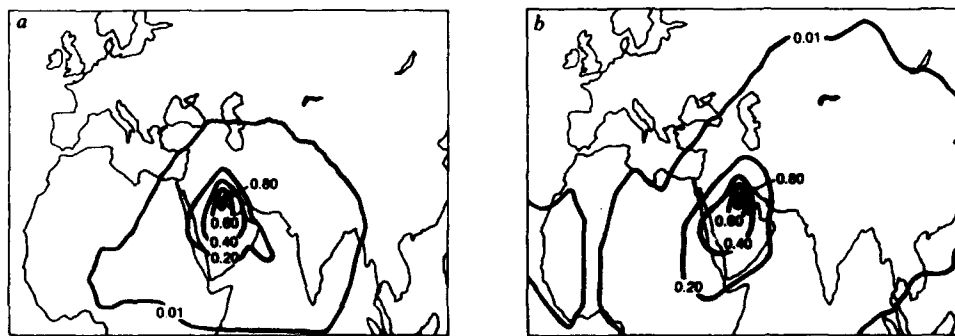


FIG. 3 Mean distribution of smoke for the period April–September derived from 10-day trajectories computed using the trajectory facility of the European Centre for Medium-Range Weather Forecasting¹⁹. The figure shows contours of the number of hours, during the 2-year period 1989–90, when trajectories, originating in Kuwait, covered various model grid squares, normalized by the corresponding number of hours over the Kuwait grid

square, for trajectories a, below 800 mbar and b, between 800 and 400 mbar. The contours may be roughly interpreted as normalized concentrations, although they exaggerate the amount of smoke at long range because they do not take into account losses by deposition. The gap and reappearance of material at longer range are due to the three-dimensional nature of the trajectories and the relatively small sample used.

The experiment and the control (with no smoke) were run from April to September. In the experiment, atmospheric solar heating in the centre of the plume increased by about 80 W m^{-2} (or 0.8°C per day), whereas the surface heating was reduced by $\sim 25 \text{ W m}^{-2}$. The surface and troposphere remained convectively coupled, so there was net heating of the troposphere-surface system which produced a slight enhancement of the Asian summer monsoon and, in most places, of the associated precipitation. This is in contrast to nuclear winter simulations in which the smoke is so thick and high that solar heating of the surface is effectively eliminated, the surface and troposphere are thermally decoupled²⁰, and there is a weakening of the Asian summer monsoon with reduced precipitation²¹.

Finally, we estimated the interannual variability of precipitation in the monsoon region, averaged over July to September, using data from existing simulations run with the observed sea surface temperatures for seven different years (1950, 1958, 1976, 1983, 1984, 1987 and 1988, encompassing wet and dry conditions in the Sahel¹⁷). The predicted changes in precipitation over southeast Asia ($5\text{--}30^\circ\text{N}$, $70\text{--}105^\circ\text{E}$) exceed twice the standard deviation of the interannual variations over only 10% of the area, and are all increases. In summary, the assumed scenario does not lead to significant decreases in the precipitation in the Asian summer monsoon, and might even lead to increases in certain regions. \square

Received 2 April, accepted 9 May 1991

1. Note placed by Secretary of State for Defence in House of Commons Lib. 17 January 1991
2. Small R D. *Nature* **350**, 11–12 (1991)
3. Briggs G A. *Plume rise* (US Atomic Energy Commission Rep No TD-25075 (US Department of Commerce, Springfield, Virginia, 1969))
4. Radia L, F. Lyons, J H. Hobbs, P V & Weiss, R E. *J. geophys. Res.* **95**, 14071–14076 (1990)
5. Golding, B W. *Meteor. Mag.* **119**, 81–96 (1990)
6. Golding, B W, Goldsmith P, Machin N A & Slingo A. *Nature* **319**, 301–303 (1986)
7. Turco R P, Toon O B, Ackerman T P, Pollack J B & Sagan C. *Science* **247**, 166–176 (1990)
8. Warren S G & Wiscombe W J. *Nature* **313**, 467–469 (1985)
9. *Nature* **360**, 96 (1991)
10. *Science* **251**, 372 (1991)
11. Pearce F. *New Scientist* **129**, 30–31 (1991)
12. Marston, R H & Smith, F B. *Österreich. Beitrage Met. Geoph.* **1**, 137–146 (1989)
13. Nicholson K W. *Atmos. Envir.* **22**, 2653–2666 (1988)
14. Jytha K. *Atmos. Envir.* **A25**, 263–270 (1991)
15. Ahmed, A F M, Singh, R P & Elmubarak, A H. *Atmos. Envir.* **A24**, 2927–2934 (1990)
16. UK Terrestrial Effects Review Group Rep. No. 1. *Effects of acid deposition on terrestrial environments in the UK* (Department of the Environment, HMSO, 1987)
17. Folland, C K, Owen, J, Ward, N & Colman, A. *J. Forecasting* **10**, 21–56 (1991)
18. Mitchell, J F B & Slingo A. *J. geophys. Res.* **93**, 7037–7045 (1988)
19. Roskilly R. *ECMWF Met. Bull.* No. 116 (1987)
20. Cess R D. *Climate Change* **7**, 237–251 (1985)
21. Ghan S J, MacCracken M C & Walton J J. *J. geophys. Res.* **93**, 8315–8337 (1988)
22. Cachier, H, Burt-Merfeld, P, Fontugne, M & Raucher, J. *J. atmos. Chem.* **3**, 469–489 (1985)
23. *Acid deposition in the UK, 1986–1988*. Third Report UK Review Group on Acid Rain (Department of Transport, South Ruislip, UK, 1990)

Printed in Great Britain by Tarrington Limited, Basingstoke, Hampshire

Airborne observations of the physical and chemical characteristics of the Kuwait oil smoke plume

D. W. Johnson^{*}, C. G. Kilsby[†], D. S. McKenna^{*}, R. W. Saunders^{*},
G. J. Jenkins^{*}, F. B. Smith[‡] & J. S. Foot[§]

^{*} Meteorological Office, Meteorological Research Flight, Royal Aerospace Establishment, Farnborough, Hampshire GU14 6TD, UK

[†] Present address: Civil Engineering Department, University of Newcastle, UK

[‡] Meteorological Office, London Road, Bracknell, Berkshire RG12 2SZ, UK

[§] Meteorological Office, Remote Sensing Instrumentation, Royal Aerospace Establishment, Farnborough, Hampshire GU14 6TD, UK

Airborne measurements in the densest part of the smoke plume at about 120 km from the burning wells in Kuwait in late March 1991 showed typical particulate mass densities of 500–1,000 $\mu\text{g m}^{-3}$, mixing ratios of 500–1,000 p.p.b.v. of sulphur dioxide and 30–60 p.p.b.v. of nitrogen oxides. One thousand kilometres from Kuwait, ozone concentrations in the plume exceeded background levels by about 50 p.p.b.v. The oil burn rate was estimated from sulphur fluxes to be 3.9 ± 1.6 million barrels per day. Significant amounts of smoke were observed only below 5,000 m altitude, and the measured attenuation of solar radiation by the smoke was similar to those assumed in recent assessments.

ABOUT 600 naturally pressurized oil wells were set alight in Kuwait in late February 1991, injecting massive quantities of smoke, sulphur dioxide (SO_2), unburnt hydrocarbons and nitrogen oxides ($\text{NO}_x = \text{NO} + \text{NO}_2$) into the atmosphere. Assessments^{1–3} of the impact of these pollutants are subject to large uncertainties in the magnitude and the characteristics of the emissions and the resulting plume. To investigate the chemical and particulate composition of the smoke, and its effect on visible and thermal radiation, the C-130 aircraft of the Meteorological Office Research Flight made 57 h of observations in eight flights into and around the plume in March 1991. Here we report

the first airborne measurements of the plume both close to the source (up to 200 km) and in the far field (1,000 km from source).

Meteorology and plume behaviour

Typically, the smoke from individual oil-well fires combined and rose so that the plume top reached ~4,500 m, often with shallow convective clouds forming on the windward edge of the plume. There was a marked vertical wind shear leading to differential advection of the plume, with, for example, the lower part of the plume being transported southeastwards down the Gulf, with the upper part moving over Iran.

There has been speculation that, because of radiative self-heating, aerosol may be lofted⁴ into the stratosphere, where its long lifetime would allow transport over considerable distances. Visual observations showed the plume top to be well defined with a maximum height of 5,000 m. On one or two occasions a detached smoke layer was seen a few tens of metres above the main top. These observations in springtime show that the smoke was confined to the lower half of the troposphere and significant amounts were not being lofted into the stratosphere, in agreement with recent assessments^{2,3}.

Particulates and chemistry in the near-field

Vertical profiles and cross-wind horizontal runs through the plume were carried out on 28 March 1991, 120 km downwind of the source (defined as 29° N, 48° E) south of Kuwait city. This distance was chosen as it was close enough to the source areas that all emissions could be measured while not so close that the inhomogeneity of the individual sources rendered the measurements unrepresentative.

A passive-cavity aerosol spectrometer probe (PCASP) was used to measure smoke particle concentrations and deduce the

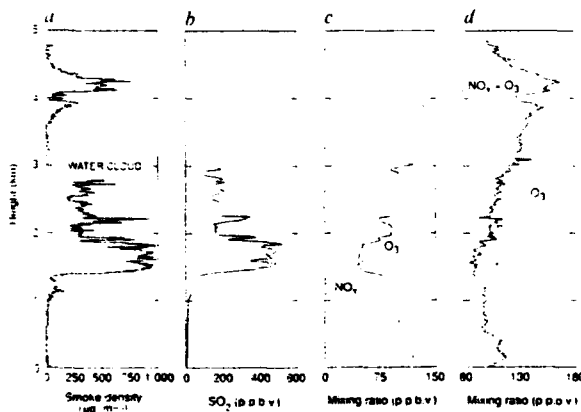


FIG. 1. Vertical cross-section of the plume made in a descending profile on 28 March 1991, 120 km from the source. *a* Smoke density ($\mu\text{g m}^{-3}$); *b* SO_2 (p.p.b.v.); *c* O_3 (solid line) and NO_x (dashed line); *d* O_3 outside the plume (solid line) and $\text{O}_3 - \text{NO}_x$ in the plume (dotted line).

ARTICLES

TABLE 1 Hydrocarbon analyses of plume samples

Species	Sample A 30 March 1991		Sample B 30 March 91		Sample C 29 March 91	
	Mixing ratio (p.p.b.v.)	Ethane ratio	Mixing ratio (p.p.b.v.)	Ethane ratio	Mixing ratio (p.p.b.v.)	Ethane ratio
ethane	25.111	1.000	5.440	1.000	1.330	1.000
ethene	13.030	0.519	1.851	0.340	0.034	0.026
propane	19.952	0.794	2.345	0.431	0.453	0.340
propene	1.637	0.065	0.220	0.040	0.026	0.020
benzene	1.057	0.042	0.215	0.040	0.044	0.033
toluene	1.309	0.052	0.203	0.037	0.025	0.019
n-hexane	5.052	0.201	0.409	0.075	0.013	0.010
NMHC	339.6	13.53	45.92	8.44	6.266	4.71

Analyses of 1.6-litre stainless steel flasks, by gas chromatography-flame ionization detector. Sample A, most polluted sample, 120 km from source; sample B, typical polluted sample at a similar distance; sample C, typical far-field sample (1,000 km from source).

mass of smoke particles per unit volume (smoke density). Continuous measurements were made of SO_2 , NO_x and ozone (O_3) with accuracies of $\pm 5\%$, $\pm 10\%$ and $\pm 5\%$ respectively. Stainless steel flasks were pressurized with ambient air and subsequently analysed for C_2 - C_8 hydrocarbons.

Figure 1 shows pollutant concentrations, together with the sum of O_3 and NO_x mixing ratios, from a descending profile carried out alongwind through the centre of the plume. Also shown is an O_3 profile obtained earlier outside the plume. The plume had a complex vertical structure, made up of two main layers: an upper one with a top at 4,600 m and base at 3,600 m, and a deeper, denser lower layer with a top at 3,200 m and base 1,000 m. The lower layer was capped by thin (200 m) altocumulus with droplets of high concentration (270 cm^{-3}) and small effective radius ($2.5 \mu\text{m}$). The upper layer was advected eastwards while the lower layer was advected southeastwards down the Gulf, trapped by a weak temperature inversion at the top of the liquid water cloud.

Seven horizontal, cross-wind runs over the same ground position were carried out at 1,420 m, 1,520 m (twice), 1,980 m, 2,440 m and 4,420 m (twice). Figure 2a-d shows measurements from a run through a 30 km-wide plume (near the centre of the

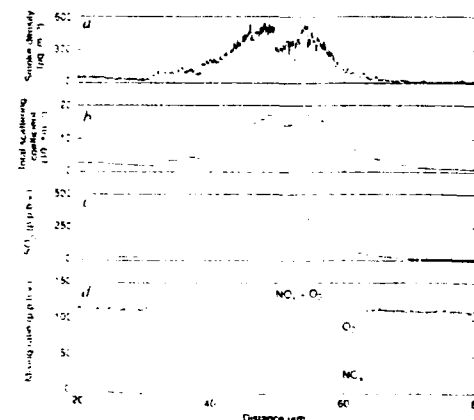


FIG 2 Horizontal cross-section through the plume at 2,440 m on 28 March 1991. a, Smoke density; b, total scattering coefficient at $0.48 \mu\text{m}$ as measured by an integrating nephelometer; c, SO_2 ; d, O_3 (solid line), NO_x (short-dashed line) and $\text{O}_3 + \text{NO}_x$ (long-dashed line).

618

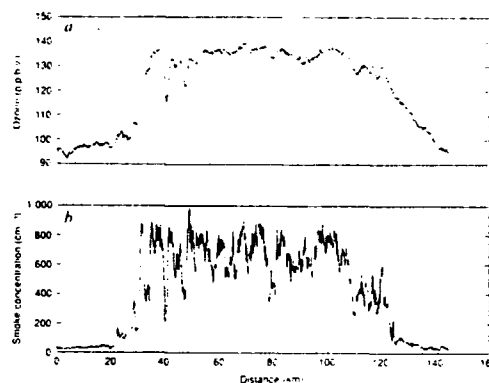


FIG 3 Horizontal run at an altitude of 4,400 m through the area of smoke (~1,000 km from Kuwait) on 29 March 1991 showing a, O_3 mixing ratio; b, smoke concentration.

lower layer at 2,440 m) of pollutants, total scattering coefficient and $\text{NO}_x + \text{O}_3$. In both the vertical profiles and horizontal runs all the plume indicators (SO_2 , NO_x , particulates and scattering coefficient) were highly correlated; this correlation was observed over several days of measurements close to the source. In the lower layer, NO_x and O_3 mixing ratios were negatively correlated, indicating gas-phase titration of O_3 by NO , but their sum showed little horizontal variation (Fig. 2d), indicating little loss of O_3 either by reactions with smoke particles or in the oxidation of SO_2 to sulphate. In the upper layer, the observed correlation between NO_x and O_3 was zero or positive, indicating that photochemical oxidant production had already been initiated.

Analyses of hydrocarbon samples taken in different parts of the plume are summarized in Table 1. The flask that showed the highest mixing ratios of hydrocarbons (sample A) was filled at an altitude of 2,600 m in the densest part of a smoke plume on 30 March 1991, 120 km from source. The aggregate of the carbon contained in all the identifiable non-methane hydrocarbons (NMHC) implies the presence of at least 340 p.p.b.v. of carbon as unburnt hydrocarbons. Assuming unidentified species having a flame ionization response are hydrocarbons, we infer a carbon content of over 460 p.p.b.v. A second flask filled on the same day (sample B) at an altitude of 1,500 m near the bottom of the plume was a more typical sample; compared with a UK urban air sample, the maximum mixing ratios of benzene and toluene in the plume sample were lower, but that of n-hexane was substantially greater.

Two supersaturation cloud condensation nuclei (CCN) spectra taken on 28 March 1991, one just below the top of the upper smoke layer at 4,500 m and the other in clear air at 5,200 m, indicate the plume contains an order of magnitude more CCN for a given supersaturation. For example, at 0.6% supersaturation, CCN concentration increased from 140 cm^{-3} to $2,000 \text{ cm}^{-3}$. In the thicker parts of the plume, CCN were so numerous ($>4,000 \text{ cm}^{-3}$) that the counter became overloaded.

Far-field measurements

On 29 March 1991, satellite images showed smoke over central Saudi Arabia, some distance from Kuwait, oriented southwest-northeast and being advected to the northeast. The O_3 mixing ratios and particle concentrations observed in a horizontal run through this area of smoke are shown in Fig. 3a and b. In this more distant plume, it is likely that the ozone, enhanced by 40-60 p.p.b.v. above the already high values in the adjacent clear air, is formed from ozone precursors (NO_x and NMHC) released

from the oil fires. Sample C (Table 1), taken in this distant plume, has a different distribution of hydrocarbons from the hydrocarbon samples collected near the fires. It still has relatively high mixing ratios of the longer-lived hydrocarbons, such as ethane and propane, but short-lived hydrocarbons such as ethene and propene are substantially reduced. The low mixing ratios of shorter-lived species suggest that considerable OH degradation has occurred, as is consistent with the enhanced ozone mixing ratio. Although the NO_x mixing ratios in the plume were below the limit of detection (5 p.p.b.v.), further ozone production remains possible because mixing ratios of only several parts per 10^{12} (p.p.t.v.) are required to generate ozone⁶. The absence of many of the more reactive and therefore short-lived hydrocarbons means, however, that further ozone production will proceed more slowly.

The observations of this mature area of smoke suggest an interpretation of some of the clear-air observations in the near field. During many of the vertical profiles made near the source region but outside the visible plume, ozone mixing ratios much greater than the normal free tropospheric background (30–40 p.p.b.v.) were encountered (for example, Fig. 1d), associated with slightly increased particle density. The enhanced ozone mixing ratios observed in the clear air were probably formed from NO_x and NMHC in smoke emitted several days earlier that remained near, or returned to, the source area.

Morphology of smoke particles

During flights in the smoke plume, ambient air was drawn through polycarbonate filters which were subsequently studied with a scanning electron microscope (SEM). Figure 4a shows a typical smoke particle from a filter exposed 180 km from the source, on 30 March 1991. The smoke particles are composed of spherules of diameter $\sim 0.1 \mu\text{m}$, which form chains of hundreds in number and several micrometres in length, as observed in other studies^{4,7}. Particles on filters exposed more than 1,000 km from Kuwait (Fig. 4b) have a different appearance from those from the near field; although the spherule size is similar in both cases, the spherules in the far field are more

TABLE 2 Estimates of strength of oil-well sources

Component	This study (Mt yr ⁻¹)	Ref. 2 (Mt yr ⁻¹)	Ref. 1 (Mt yr ⁻¹)	Ref. 3 (Mt yr ⁻¹)
Total burn rate	202.5	80	63	161
Carbon as gas	161.2*	60	63	—
Fine carbon particulate	6.4†	5	5.8	16.1
Sulphur	6.1‡	2	—	—
Nitrogen in oxides	0.42*	0.5	—	—

Estimates derived from observations and, for comparison, those assumed by recent assessments^{1–3}. The mass of hydrogen contained in H_2S and hydrocarbons in the fuel has been taken into account when determining the different components of the emissions.

* Deposits from large partially burned oil droplets near the well heads may reduce this total.

† Assuming the same emission factors for the southern and northern fires.

‡ This quantity could be up to 2–3 times higher with a commensurate reduction in carbon as gas.

§ Assuming a 1.5% sulphur content for the northern fields which contribute 15% overall to the emissions.

likely to be closely packed into near-spherical clusters. Similar behaviour has been noted⁸ in laboratory experiments, in air aged at high humidity.

The PCASP determines the number and size distribution of particles by passing them through a laser beam and measuring the scattered light intensity, using a relationship between intensity and size derived from experiments with latex spheres of known radius. The smoke density is calculated by integrating the size distribution assuming (1) that collection efficiency is 100%, (2) that the nonspherical particles in the plume scatter the same amount of light as spheres of the same mass (we conclude from previous experimental⁷ and theoretical⁹ work that, for the particle shapes encountered, this assumption is reasonable) and (3) that the density of the smoke particles is 1 g cm^{-3} , in line with Sokolik¹⁰. Support for this approach comes from the mass loading of the filter samples, which indicate that the absolute determination of smoke density from the PCASP is not grossly in error, and from the linear relationship between

FIG. 4 Scanning electron micrographs of smoke particles collected on filters exposed in the plume on a. 30 March 1991, 180 km from the source, and b. 29 March 1991, $\sim 1,000$ km from the source. The filters were mounted on an extendible boom 0.4 m from the aircraft skin and the air sampled isokinetically¹⁴. The dark holes in the photograph are the pores in the filter.



ARTICLES

SO₂ concentrations and smoke density (see below) which confirms that the instrumental response to smoke density is linear. Nevertheless, the uncertainties in these assumptions lead us to believe that the absolute values of smoke density could be up to 2-3 times as high as those shown. The relative variations in the plots are still valid.

Emission estimates

The amount of sulphur emitted was estimated from the flux of sulphur through a crosswind plane, determined from the product of sulphur concentration and the wind component perpendicular to the plane. Sulphur dioxide measurements from the horizontal runs and vertical profiles through the plume were used, together with the winds measured by the aircraft. Above 3,000 m, where the SO₂ monitor will not operate, PCASP measurements were used to derive proxy SO₂ values through the linear relationship evident in Figs. 1 and 2.

On 28 March 1991, when virtually all the plume ~120 km from the southern oilfields was sampled, the estimated sulphur emissions were 5.7 Mt yr⁻¹. Assuming a value of 3.3% for the sulphur content of the southern oilfields (R. D. Small, personal communication), this source strength corresponds to an oil burning rate of 172.1 Mt yr⁻¹. We assume, based on previous estimates^{11,12}, that the southern oilfields account for 85% of the total burning rate; this implies a total rate of 202.5 Mt yr⁻¹ or 3.9 × 10⁶ barrels per day. An estimate for 30 March 1991 gives a similar burning rate. Our subjective estimate of the error in this source strength, based on the temporal evolution and spatial variability over the 3 h measurement period, is ~40%.

Using the relationships between concentrations of SO₂, NO_x and particulates, we estimate the source strength of NO_x and particulates from the sulphur source strength (Table 2). Carbon

as gas (the mass of carbon contained in CO, CO₂, CH₄ and NMHC) is estimated from the residual mass after the mass emissions of sulphur, nitrogen and particulate carbon are subtracted from the total mass emitted and an allowance is made for the hydrogen content.

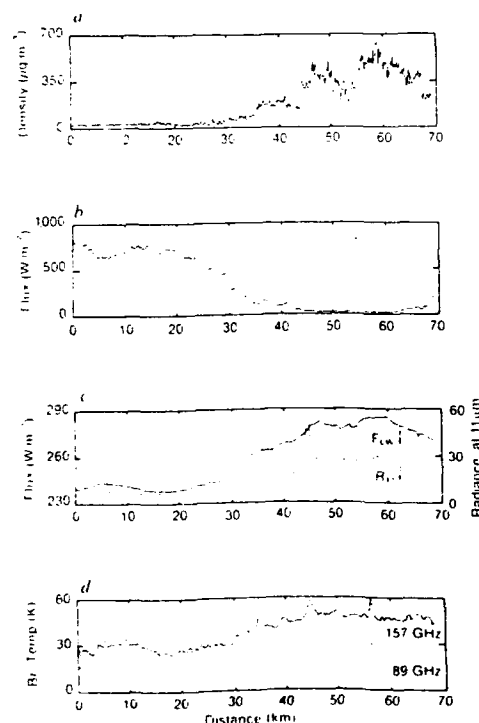
Effect of the smoke on radiation

Figure 5 shows the effect of the smoke on the radiation during a horizontal run on 31 March 1991 through the centre of the plume, 700 m below its top, ~65 km from source. The total shortwave (0.3-3 µm) downwelling flux was reduced from its clear-sky value of 800 W m⁻² outside the plume to zero in the centre, and corresponding changes were seen in the infrared and microwave regions.

The single scattering albedo, ω_0 , of the smoke was estimated in two independent ways. First, we measured hemispheric reflectances of the plume, ρ_{up} , using upward- and downward-looking pyranometers, to be 5-8% over a range of solar zenith angles (25°-48°). The Ginzburg and Sokolik¹³ method shows that these reflectances correspond to a value of ω_0 in the range 0.5-0.55, but with an uncertainty of ±0.1 because of assumptions made about the scattering properties of oil smoke. Second, we measured volume absorption coefficients from filters exposed in the plume using the integrating sandwich technique¹⁴, and these, when combined with the nephelometer scattering coefficients, give values for ω_0 in the range 0.55-0.70 (±0.1). Thus the likely range of ω_0 is 0.50-0.65, which is higher than previously published values for oil smoke^{4,7,10} but lower than that of 0.8-1.0 measured in non-carbonaceous aerosols¹⁵.

The broadband optical depth of the smoke was estimated from the change in downwelling shortwave flux as the aircraft ascended or descended through the plume. Figure 6 shows the

FIG. 5 Illustration of the effect of the smoke on downwelling radiation during a crosswind run through the centre of the plume. a. Smoke density, b. shortwave flux, c. infrared flux F_{IR} and radiance at 11 µm, R_{11} , (in units of mW m⁻² steradians⁻¹ (cm⁻¹)⁻¹), d. the zenith microwave brightness temperatures at 89 and 157 GHz.



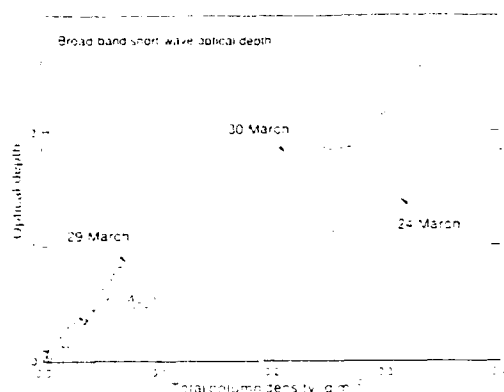


FIG. 6 Broad-band short-wave optical depths of the plume from three different ascending or descending profiles flown through the plume as a function of the total column density of smoke in the path. The profile on 29 March 1991 was further away from the source and lower smoke densities were encountered.

derived optical depth as a function of smoke column density for three profiles through the plume top. Solar heating rates in the plume were calculated from shortwave flux divergences in a profile at local noon on 30 March 1991, 140 km from the source. The heating rate was typically $\sim 50 \text{ K d}^{-1}$ throughout the depth (2,300 m) of the smoke. It was nearly constant in the plume because the smoke density increased from the top to the base. At a distance of 250 km from the source, the smoke density was a factor of four lower and the heating rates were 20 K d^{-1} . This compares with typical clear-sky values of 1 K d^{-1} .

Figure 5c shows the downward hemispheric infrared (4–50 μm) fluxes to be 45 W m^{-2} greater in the centre of the plume than in clear air and the vertical downward radiance at 11.1 μm to be increased by $20 \text{ mW m}^{-2} \text{ steradians}^{-1} \text{ cm}^{-1}$. These were measured by a pyrgeometer¹⁵ and a narrow field of view (1.5°) radiometer¹⁶ respectively. The peak in radiance at 45 km along the run is probably due to cloud above and is also seen in the microwave measurements (Fig. 5d). The broadband infrared optical depth for a vertical path through the smoke was calculated in a similar manner to the visible optical depth. It was estimated to be 0.34 ± 0.05 for the profile on 30 March 1991. The 11.1- μm radiometer was not operated in this profile, but the maximum vertical optical depth calculated from the horizontal run in Fig. 5c was 0.30 ± 0.02 , which was 75% of the corresponding broadband optical depth. The infrared cooling rate in the plume was calculated from the flux divergences to be 2.1 K d^{-1} , which is 1.0 K d^{-1} greater than that in adjacent clear air. Assuming smoke densities based on the PCASP measure-

ments, we used the optical depth to deduce a visible extinction coefficient of $7\text{--}13 \text{ m}^2 \text{ g}^{-1}$, which agrees broadly with other measurements of oil smoke¹⁷. The 11.1- μm infrared absorption coefficient was deduced to be $0.7\text{--}1.3 \text{ m}^2 \text{ g}^{-1}$, in agreement with laboratory measurements¹⁸.

Figure 5d shows the effect the plume had on downward radiances (or brightness temperatures) at 89 and 157 GHz, measured by a microwave radiometer. Atmospheric emission at these frequencies is principally controlled by water vapour and liquid water. The increase in brightness temperature in the plume at 157 GHz (22 K) is three times the increase at 89 GHz (8 K), but both are well correlated with the infrared radiance. This correlation was seen on several occasions when there was no trace of liquid water in the plume. The microwave radiance increase is surprisingly high and cannot be explained by variation in water vapour within the plume nor by the observed levels of SO_2 . Measurements¹⁹ of the absorption coefficient of diesel soot at 94 GHz are over an order of magnitude too small to account for our results.

Discussion

Our best estimate of oil burning rate is greater than those previously assumed^{1,2}. The greater CO_2 emissions that this implies, however, represent only 3% of total annual fossil-fuel emissions and would still have a negligible effect on global climate through the greenhouse effect. The sulphur emissions calculated are considerably higher than those taken by Browning *et al.*², and although we would expect the acidity of rainfall episodes to be no higher than previously predicted, because it is limited by droplet saturation, these episodes will extend further downwind across southern Asia. As predicted², increased photochemical oxidant concentrations were observed both close to the source and further afield. But the emissions of NO_x are smaller than those previously assumed², for this reason and because they are rapidly removed, they are unlikely to influence the global NO_x background or global tropospheric ozone.

The estimated smoke emission rate, even with our large uncertainties, is similar to the range used in previous assessments^{1,2}. Furthermore, the product of our derived visible extinction coefficient and smoke emission rate (the factor that determines the radiative impact of the plume for a given meteorological situation) is independent of the uncertainties in our estimate of smoke density and is similar to that inferred from Browning *et al.*². Previous assessments^{1,2} assume that the smoke did not scatter radiation; the scattering that we observed would be insufficient to alter their conclusions significantly. The observed infrared effects, although previously ignored, will only very slightly ameliorate the predicted daytime surface cooling. Our measurements thus confirm the assumptions used in recent assessments^{1,2}, and the observation that significant amounts of smoke were not present above 5,000 m bears out their predictions. This study provides strong support for their conclusions that, although the effects may be significant on a regional scale, those on a global scale, including the Asian summer monsoon, are likely to be insignificant.

Received 14 June; accepted 17 September 1991

- Small, R. D. *Nature* **350**, 11–12 (1991).
- Browning, K. A. *et al.* *Nature* **351**, 363–367 (1991).
- Balan, S. *et al.* *Nature* **351**, 367–371 (1991).
- Ridley, L. F., Lyons, J. H., Hobbs, P. V. & Weiss, R. E. *J. geophys. Res.* **95**, 14071–14075 (1990).
- Marsh, A. P. W., Crutcher, J. & Harrison, D. B. CERL RD/L/2092/81. Central Electricity Research Laboratories (Leatherhead, 1982).
- Crutcher, J. *J. Tropospheric Ozone* **3**, 32 (Reidel, Dordrecht, 1988).
- Corbett, J., Hardman, E. J. & Harrison, R. M. *J. Aerosol Sci.* **20**, 765–774 (1989).
- Corbett, J., Aoshov, L., Hardman, E. J. & Harrison, R. M. *J. Aerosol Sci.* **21**, 527–538 (1990).
- Berry, M. J. & Percival, J. C. *Opt. Acta* **33**, 577–591 (1986).
- Sokolov, N. *Nucl. Atmos. Ocean Phys.* **24**, 200–204 (1988).
- World Meteorological Organization Rep. ROP 554. Meeting on atmospheric part of UN response to Kuwait oil field fires, 27–30 April 1991 (WMO, Geneva, 1991).
- Environmental Impact of Oil Burning in the Kuwait Oilfields: a Preliminary Evaluation. King Fahd University of Petroleum and Minerals, Dhahran (1991).

- Ginzburg, A. S. & Sokolov, N. *Nucl. Atmos. Ocean Phys.* **25**, 1007–104 (1989).
- Aoshov, L. G. *J. Atmos. Sci.* **47**, 1173–1192 (1990).
- Fox, S. *J. Atmos. Ocean Technol.* **3**, 363–370 (1986).
- Rawling, F. & Fox, S. *J. Atmos. Sci.* **47**, 2488–2503 (1990).
- Jonsson, G. S., Shukurov, A. Kh., Ginzburg, A. S., Sulugin, A. G. & Aronov, A. V. *Nucl. Atmos. Ocean Phys.* **24**, 163–168 (1988).
- Roesler, D. M. & Fawcett, R. *J. Opt. Soc. Am.* **69**, 1699–1704 (1979).
- Bruce, D. N., Stromberg, P. F., Burton, A. T. & Mozer, J. B. *Radio Sci.* **30**, 1537–1546 (1991).

ACKNOWLEDGEMENTS. We thank the Royal Air Force aircraft and ground crew, RAF Muharraq, for facilities, the Mobile Met. Unit for forecasts, T. Marsh and P. Anwar of National Power Technology and Environment Centre for the use and calibration of chemical monitors, P. Brookes of RAF Muharraq, P. Aviation Medicine, C. Gamble of RAF Veterans Department for SEM photographs, RAF Aircraft Department and RAF Muharraq for aircraft maintenance, and the scientists and technicians at the Meteorological Office for their hard work and commitment. The co-operation of Sheikh Essam Abdullah Alkharaj and the State of Bahrain Ministry of Development and Industry and that of the Gulf states who granted permission for the aircraft to operate in the KRA is essential.

THE ESTIMATION OF THE OPTIMAL NUMBER OF PARTICLES REQUIRED FOR A
REGIONAL MULTI-PARTICLE LONG RANGE TRANSPORT AND DISPERSION MODEL

R. H. Maryon

Meteorological Office
Bracknell,
Berkshire, UK

1. INTRODUCTION. Simulation of the evolution of the Chernobyl plume over the 10 or more days of the release highlighted the influence of the changing meteorology in distorting the plume and dispersing material over extended periods. If a complex plume of this type is to be simulated by a Lagrangian Monte Carlo technique—that is, by the release of very large numbers of 'particles' into the model atmosphere at source, and allowing the model winds and turbulence parametrization to effect the spread—the question arises: how many particles is it necessary to release in unit time to simulate the plume adequately? It is 'obvious' that the more particles released, the greater the accuracy. However, even with modern computing facilities there are constraints upon the number of particles it is practicable to utilise: if N particles are released every hour the model will be advecting $240N$ at the end of 10 days' continuous release, with potentially very high storage and CPU requirements. On the other hand, excessive economies in the number of particles released may result in a totally inadequate plume simulation. What is the optimal configuration?

Theory can help a little, but does not provide a clear answer in situations of great complexity. For example, a standard result used for Lagrangian particle models is that, in a given grid-cell,

$$A = \frac{\sigma_c}{c} = \left(\frac{Q}{NVc} \right)^{1/2} \quad (1)$$

where c is the 'real' concentration in a grid-cell, Q is the mass of material released, V is the grid-cell volume (taken as constant in this paper) and σ_c is the standard deviation of the estimate. Thus the ratio A is a measure of accuracy (the coefficient of variation), which is proportional to both $N^{-1/2}$ and $c^{-1/2}$; for a given value of A , N is obtainable from c , or vice versa. Vc/Q in (1) can be interpreted as the expected fraction of particles in a grid-cell and the complete term in brackets the reciprocal of the expected number of particles. From (1)

$$\frac{\partial A}{\partial N} \propto N^{-3/2},$$

confirming rapid improvement of accuracy with particle number at small N but only a slow improvement at large numbers.

Expression (1) is derived from elementary probability theory, and uses the initial assumption that the probability of a particle occurring in a grid-cell is m/Q , where m is the

'real' mass occupying the grid-cell. In other words, (1) supposes that the diffusion of the plume is being accurately modelled. 'Real' here, is taken as a definitive simulation or 'validation' produced by a Monte Carlo model using an indefinitely large number of particles. Thus there is a 'correct' number of particles occupying each grid-cell, which may be expressed as a ratio of the total number of particles released.

Now with Monte Carlo models, diffusion is effected by a random forcing, or, for long range transports, quite adequately by a random displacement of the type

$$\mathbf{x}_{t+1} = \mathbf{x}_t + \mathbf{u}(\mathbf{x}_t)\Delta t + \sqrt{2\Delta t K} \mathbf{r} \quad (2)$$

where \mathbf{x}_t is a displacement vector at time t , \mathbf{u} the wind velocity, K a diffusivity and \mathbf{r} a random number generated from a suitable distribution. Diffusion will not necessarily be modelled consistently, here, for extended releases, as different realizations of the random walk will lead to relative, local, differences in particle density, which will be acted upon by the evolving synoptic wind pattern. Indeed, different realizations of the diffusion process are being coupled with what is well known to be a chaotic system. The local differences will be accentuated with the passage of time. Thus simulations of a complex plume using relatively few particles will lead to somewhat different configurations from the hypothetical validation, and from each other. The object of this exercise is to estimate the number of particles required to remove serious error due to these effects. Expression (1) tells us little about the size of N required to model a complex situation: near the fringes of the plume c will be indefinitely small, and with Q most likely unknown it is very difficult to arrive at a sensible estimate for N . A value for A must be decided upon, and even a choice of a threshold value for c will be species-dependent, and may be difficult to prescribe *a priori* in cases of, say, nuclear accident. If c and Q are ignored, and attention is confined to the spread of particles, the difficulty arises of defining what constitutes an acceptable level of error.

A straightforward way of estimating the number of particles required adequately to simulate a complex plume of many days' duration is to carry out sensitivity studies leading to an empirical result. To do this properly, very powerful computing facilities are needed, enabling a simulation using an 'indefinitely large' release of particles to be used as validation. It is to be hoped that the prior assumption of the adequacy of the control, for a period at least, after release, will be confirmed in the course of the investigation. Note that we are not, here, trying to estimate how many particles are needed for a correct answer in any absolute sense, as no model is capable of producing such, but can only provide an approximation which depends upon the conditions, the model configuration and parametrizations. What we are trying to do is to find the most economical configuration which produces a solution which is not significantly different from the 'best' answer that the multi-particle model is capable of producing.

2. THE MODEL. The model used is the U.K. nuclear accident response model, acronym NAME, a Lagrangian 3-dimensional multi-level, multiple particle model of which a brief preliminary description is contained in Maryon and Smith (1989). The model winds and other meteorology are obtained from the U.K. Met Office operational 'Limited Area' NWP model. The lowest analysed level is the atmospheric boundary layer, which is derived from the NWP profiles, and of variable depth. The upper model levels, and indeed its grid, correspond to that of the underpinning NWP model. The resolution is 0.4425 deg both lat and long, but the coordinates are rotated so that Europe benefits from the relatively uniform mesh of Equatorial regions.

Particles are transported by the model winds, including the analysed vertical component. A 10m wind is diagnosed which is consistent with Monin-obukhov similarity theory. All wind components are zero at the surface. Sub-grid turbulence is simulated by the addition of a random component as in (2): in addition, at each timestep (15 min—roughly the eddy

turnover time for the convective boundary layer) all the particles *below the capping inversion* are randomly reassigned in the vertical, within the boundary layer. Horizontal and vertical diffusion are reduced above the inversion. The meteorological fields from the NWP model, and the rainfall rate, which is drawn from various sources, notably radar, are archived over a 10-day period, and are continually updated. The model has many features which cannot be described in the space available here: it is hoped to publish a fuller description shortly.

3. EXPERIMENTAL METHOD. The investigation was carried out using the NAME model on the U.K. Met Office Hitachi EX100 mainframe computer. The 10-day roll-over archive was 'frozen' at a convenient time so that repeated integrations could be carried out using identical meteorology. This archive alone required nearly 300 Mbytes of storage.

For the present study all particles were released from a reasonably central point 50 deg N 20 deg E, from a notional source in the boundary layer, the release commencing 12GMT 23rd June 1991. Plots of the particle spread show that over the 10 days some drifted out of the domain and are lost to the analysis. Many others, of course, were lifted to high levels. The particles remaining below 900 mb were used in the calculations for this study, to avoid the processing of very large numbers of grid-cells, and to concentrate on the critical near-surface particle densities. There is no compelling reason to assume that a full 3-dimensional analysis would greatly alter the results, however.

The following validation runs were made:

Exp A: 4000 particles/hr released for 144 hr, the integration continuing up to 240 hr.

Exp B: as Run A, but 6000 particles/hr released.

Exp C: 12000 particles/hr released for 72 hr, the integration continuing up to 240 hr.

It is taken on trust, for the moment, that some or all of these runs do in fact constitute an adequate validation. The maximum computer core used was 38 Mbytes and the longest integrations extended over 9 hr CPU time—despite the fact that in the interests of economy no calculations of concentration (as opposed to particle counts), radioactive decay or wet and dry deposition to the surface were made. These latter diagnostics are all dependent on concentration, and if calculated may be expected to reflect only the shortcomings of the particle densities, which are to be analysed here.

Identical meteorological data were employed for trial integrations corresponding to Exp A, B and C using releases of 2,4,8,16,32,64,128,256,512, 1000,2000,3000... particles/hr, culminating in a release of similar size to the validation but using a different realization of the random walk (2). It was not deemed necessary to include all the larger integrations for Exp C, however.

4. ANALYSIS OF RESULTS. A suitable statistic for representing the error of the trial runs is

$$S = \left\{ \sum_i \left(\frac{n_{ib}}{tN_b} - \frac{n_{ia}}{tN_a} \right)^2 \right\}^{1/2} \quad (3)$$

where i sums over all bottom layer grid cells, n_{ia} , n_{ib} are the numbers of particles in grid-cell i for releases of N_a , N_b particles/hr, over a period of t hr, where subscripts a , b indicate the validation and trial runs respectively.

A digression: the χ -square statistic. It was noted that statistic S is not far removed from a χ -square statistic, if it is assumed that the grid-cell contents of the validating runs constitute an 'expected distribution' of the particles. For air concentration a suitable statistic can be defined

$$\chi_c^2 = \sum_i \frac{(c_{ib} - c_{ia})^2}{c_{ia}}$$

with the RHS subscripts as in (3). In terms of the particle analysis this becomes

$$\chi_c^2 = \frac{Q}{tN_a V} \sum_i \frac{(Rn_{ib} - n_{ia})^2}{n_{ia}}$$

if V is constant. Here, R is the ratio N_a/N_b . It is not practicable to use this formula, which is a function of Q . However the summation

$$\chi_p^2 = \sum_i \frac{(Rn_{ib} - n_{ia})^2}{n_{ia}} \quad (4)$$

is a closely related χ^2 statistic where Rn_{ib} is the weighted number of particles in the trial grid-cells—we are saying, in effect, that each trial particle corresponds to R of the validation particles, which in the trial runs are forced to 'adhere' due to the loss of degrees of freedom where fewer particles are available. Thus in (4) we compute the squared difference between this weighted number of trial particles and the number of validation particles in the grid-cells.

A χ^2 test might now be cast entirely in terms of particle numbers, without dependence on unknowns such as Q . The degrees of freedom, ν , of the χ^2 test is taken as the number of grid-cells occupied by 5 or more particles of the validating plume; those with 4 or less are combined in one 'bin'. One possible level of significance for the test is 50%, for which, at random, half the acceptable realizations would have $\chi_p^2 > \chi_{50}^2$. The degrees of freedom for such a test greatly exceed the values usually published in table form, but to a close approximation,

$$\chi_{50}^2 \approx \nu \left(1 - \frac{2}{9\nu}\right)^3 \quad (5)$$

(see Dixon and Massey, 1969; for other significance levels the formula has an additional term requiring the normal deviate). Clearly, as $\nu \rightarrow \infty$, $\chi_{50}^2 \rightarrow \nu$. This limit applied to (4) leads to the interesting deduction that in individual cells i we are looking for

$$n_{ia} - \sqrt{n_{ia}} < Rn_{ib} < n_{ia} + \sqrt{n_{ia}} \quad (6)$$

(to a rough approximation), or transposed for air concentration

$$\frac{n_{ia}}{N_a} - \sqrt{\frac{n_{ia}}{N_a} \frac{V}{Q}} < \frac{n_{ib}}{N_b} < \frac{n_{ia}}{N_a} + \sqrt{\frac{n_{ia}}{N_a} \frac{V}{Q}}$$

for a successful trial.

Are the validations inadequate? Fig 1 is a plot on logarithmic axes of χ_p^2 against the number of particles released/hr for Exp B. The three curves correspond to the situation at 72, 144 and 240 hr into the integration; the continuous release, it will be recalled, extended to 144 hr. The approximation of the curves to straight lines of unit slope is noteworthy. The plots imply $\chi_p^2 \propto 1/N$ —interpreting (4) as a form of squared error this is a clear manifestation of the $N^{-1/2}$ regime discussed earlier.

Where this relation holds the error due to restricted particle numbers is predominant.

However, as the particle numbers increase, the slopes, at first imperceptibly, and towards the extremity more noticeably, depart from unity (the left hand extremes, where the plume is crudely discretised by a handful of particles, need not concern us). Where very large numbers of particles are employed, the decrease in the reduction of error with number reflects the influence of different realizations of the diffusion process (2). Whichever validation we look at, and however many particles are utilised, a departure from unit slope occurs for this reason. This decrease in error reduction prevents any close approach of χ_p^2 to χ_{50}^2 (or any other of the

commonly used significance levels) even where a trial uses as many particles as the control run (but in a different realization). $\text{Log}\chi_{30}^2$ for the three curves lies between 2.48 and 3.49: if the unit slope sections of the curve are produced to intersect these values the ordinate corresponds, roughly, to the numbers of particles released in the validation. This is no doubt due to the fact that χ_{30}^2 and the number of particles released are both closely related to the number of grid-cells covered by the simulated plume.

The implication here is that, in these validations and trials, the more particles released the more grid-cells were covered, which leads us to question the adequacy of the validations. Indeed, plots of the proportion of validation grid-cells covered against the number of particles released in the trials (e.g., Fig.2 for Exp C) fail to show (at least at 144 and 240 hr) the levelling off for large numbers of particles which would be expected if the validating runs were adequate, and the trials with many particles reasonable approximations thereto. Again, plots (not shown here) of mean proportionate error defined

$$\left\langle \frac{|Rn_{ib} - n_{ia}|}{n_{ia}} \right\rangle \quad (7)$$

(where the angle brackets imply an average over the ensemble of grid-cells) likewise fail to asymptote sufficiently as the validating particle numbers are approached, except perhaps at 72 hr, and this only close to the validation.

At first sight these seem discouraging results. However, where a random walk is applied to many particles, some, after a number of timesteps, will be displaced a considerable distance from the mainstream. The ensemble of accumulated displacements will take the form of a Gaussian distribution, and where extremely large numbers of particles are deployed, some displacements will, due to the accumulation of random effects, spread further and further into the tails of the distribution. The more extreme displacements may eventually come to represent a virtually insignificant proportion of the ensemble, but will be reflected in Fig.2 because some of them will spread into fresh grid-cells, and in the proportionate error because grid-cells containing very few particles will carry a disproportionate weight in expressions such as (7) (via its denominator). A similar argument applies to expression (4), the χ^2 statistic.

Now with extremely large numbers of particles a simulated plume can expand almost indefinitely: thus in (2), with a timestep Δt of 15 min and a diffusivity K set at $6000\text{m}^2/\text{s}$ (if anything set slightly on the large side for this project so as to avoid underestimating minimum particle requirements) those particles repeatedly being displaced by near-maximum values of r will move about 3km from the mainstream at every timestep. As a fraction of the total numbers released, the number of particles reaching such peripheral grid-cells would be negligible. The tails of the Gaussian distribution in typical short range dispersion simulations are taken as representing very uncommon effects of the turbulence or meandering which may occur in different realisations. For a specific long range transport situation, analogous extremes will occur in innumerable places, but do they occur all around the plume at all times and in all directions? It is likely that parametrisations such as (2) are not everywhere realistic when applied to a single realization, or at least that in reality the spread of material is totally insignificant in many of these grid-cells. The fixed diffusivity used here will itself be unhelpful, while the release of very large numbers of particles may even exacerbate the situation. Parametrising K as a function of the meteorology or conditions may help, but would not solve the problem. It is concluded, then, that diagnostics such as Fig.2 and expression (7) should not unquestioningly be taken as appropriate for the problem in hand.

Some empirical support. It was thus necessary to adopt a different approach, returning to the point of departure, the error statistic S , defined in (3). Figs.3a, 3b show plots of S against log of particle number for the experiments A and B. It will be observed that differences are very slight up to $n_0 = 4000$ —that is, error for a validation of 4000 particles/hr is very close

indeed to that for 6000, even after 240 hr simulation. The largest errors in Fig.3 are attached to the 72 hr integrations, no doubt because of the relatively large values of n_{ia} and n_{ib} which can occur at relatively small times. Normalising S by reference to the validating runs defines a statistic T :

$$T = S / \left\{ \sum_i \left(\frac{n_{ia}}{tN_a} \right)^2 \right\}^{1/2} = \left\{ \frac{\sum_i (Rn_{ib} - n_{ia})^2}{\sum_i n_{ia}^2} \right\}^{1/2} \quad (8)$$

plotted in Fig.4 for Exp B. It is apparent that this normalised error increases with time into integration, especially for transports following the cessation of the release, when the statistics no longer benefit from the near-source plume. Differences between plots for runs A and B are virtually indiscernible up to $n_b = 4000$, for this statistic.

The diagnostic

$$R_n = \frac{RMS(n_{ib}/N_b)}{RMS(n_{ia}/N_a)}, \quad (9)$$

is also of interest in that the ratio for a perfect simulation would be unity, and it demonstrates the rate at which the trials approach a good representation of the characteristic scatter. This is illustrated in Fig.5 for run C. The curves for runs A and B converge marginally more quickly, if anything, and again are near-identical up to 4000 particles/hr. It is necessary to take care in interpreting some of these statistics: the rate at which these curves converge gives an erroneous impression of the number of particles necessary to give an adequate simulation.

The near identity of runs A and B for statistics R_n and T and (most importantly) the strong similarities of these runs for the unmodified error S imply that 6000 particles/hr should constitute an adequate validation for the situation modelled, contrary to the impression given by Figs.2 and 3 where the results are influenced by fringe effects of questionable significance.

To check on the significance of these peripheral effects a count was made of the average number of particles in those validation grid-cells which the trials failed to reach. These values are plotted in Fig.6 for run C, for example, with the control release of 12000 particles/hr (for 72 hr). This, for the most part, underlines the minute number of particles contained by these peripheral cells: a cell with ten particles holds less than 0.1% of an hour's release, in a region which might well not be affected in reality. Of course, a minority of cells will contain considerably more than the average: for example, modelling the 240 hr plume of run C with 512 particles left no less than 60% of the validation cells unreached (Fig.2); of these 10 cells contained 40 - 50 particles, 8 cells 51 - 61 (the maximum), but the overall average was 5.86 particles/cell. What proportion of this very wide diffusion was realistic?

A further point to note, here, is that the more trial particles released, the more grid-cells are reached which were not occupied in the validation (although they would have been in a hypothetical simulation with an indefinitely large number of particles!). These effects are relatively insignificant.

5. ESTIMATING OPTIMAL PARTICLE NUMBERS. It remains to make some estimate of the optimal release in the given set of circumstances, although it must be emphasised that there is no perfect or absolute answer to the problem. Two further diagnostics were calculated:

$$S_1 = \frac{1}{S} \frac{dS}{dn} \simeq \frac{S_n - S_{n+1}}{S_{n+1} \Delta n} \quad (10)$$

and

$$S_2 = \frac{S_n - S_q}{S_q \Delta n}. \quad (11)$$

In these expressions the S terms on the RHS are as in (3) with the subscripts referring to consecutive trials (see Section 3) or, for sub(q), the final trial, which uses a similar number

of particles to the validation but with a different realization of the random walk. Thus S_1 represents the proportionate decrease of error with particle number between consecutive trials, S_2 the proportionate decrease of error between individual trials and that of the equi-particle realization (an 'irreducible error'). S_1 is plotted in Fig.7 against the mean of n and $n+1$ (and in Fig.8 S_2 against the mean of n and q), and for plotting purposes expressed as percentage improvement per release of 10 particles/hr.

These plots are notable for the degree to which the curves for the different periods of integration coalesce. Fig.7 suggests that the improvements obtainable after the 512/1000 particle step are very slight. The strong vertical in Fig.8 is to be expected, as the abscissa changes little for trials releasing few particles. Nonetheless, this somewhat unorthodox abscissa highlights, at the particularly sharp bend in the curve, the stage at which increasing the particle numbers produces decreasing dividends in accuracy. The implication of all the diagrams from Fig.3 onwards, and of a number of other diagrams and statistics for which there is no room here, is that, given that a reasonable validation for integrations of 72 up to 240 hr was obtained, the rate of improvement is rather small for increases beyond 500 particles/hr, although Fig.5 suggests that 1000 particles/hr, if feasible, is distinctly preferable. The rate of improvement is very small after 1000 particles/hr. Of course, the very nature of the plume changes between 72 and 240 hr, and these effects are not always apparent in the statistics: attainable accuracy reduces with time. If improving computer capabilities enable the deployment of larger numbers then so much the better, but the present exercise suggests that improvements in accuracy will be marginal, and eventually constrained by the workings of the diffusion parametrization. The use of a fixed (and rather large) diffusivity in this investigation was not, with hindsight, helpful.

Choosing a threshold value for particle number, below which a grid-cell is ignored for the purposes of the investigation, would lead to an interesting reappraisal of the χ^2 test discussed earlier. This would again, however, require an *a priori* decision as to realistic spread, and is not pursued here.

Obviously the statistics derived here are situation-specific, depending on the period of the release, and particularly the presence or absence of denser concentrations around the source. The meteorological conditions may be important, particularly if the situation is changing rapidly, or there are strong vertical velocities involved. Reruns of this study with other model configurations, release scenarios and meteorology would naturally be desirable, but it is felt may not change the conclusions significantly. A useful mode of operation, in practice, may be to split particles after a certain lapse of time, utilising the computer storage of particles which have drifted out of the domain.

ACKNOWLEDGEMENT. Some interesting and helpful discussions on this topic were held with my colleagues Drs D.J.Thomson and F B Smith.

REFERENCES

- Dixon, W.J. and Massey, F.J. (1969) *Introduction to Statistical Analysis*, McGraw-Hill Book Co, New York.
- Maryon, R.H. and Smith, F.B. (1989) 'The development of the U.K. operational multi-particle transport and dispersion model', *Österreichische Beiträge zu Met. und Geoph.*, 1, 137-145.

FIGURE CAPTIONS.

Fig.1. Exp.B: A plot on logarithmic axes of χ^2_p against the number of particles released per hour for the trials. The 72, 144 and 240 hr integrations are distinguished by circles, crosses

and dots respectively. This applies to all the diagrams, which also all have identical abscissae.

Fig.2. Exp.C: percentage of validation grid-cells reached by the trial integrations plotted against the log of the number of particles released/hr.

Fig.3. Error statistic S as defined in (3) plotted against log of particle number: (a) Exp.A (4000 particle/hr validation), (b) (6000 particle/hr validation).

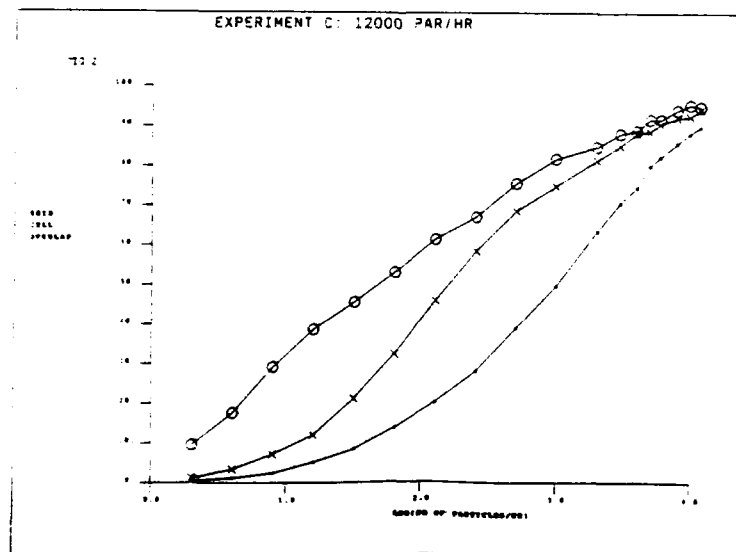
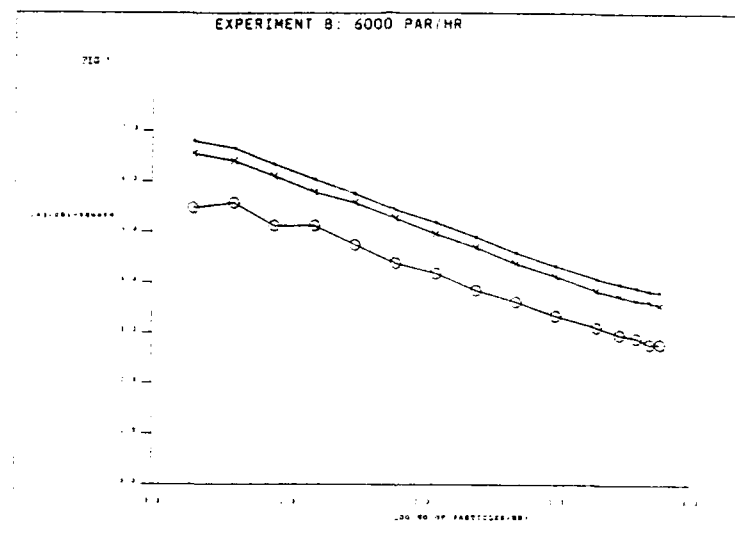
Fig.4. Exp.B: Normalised error as defined in (8) plotted against log of particle number.

Fig.5. Exp.C: Ratio of RMS errors, expression (9), plotted against log of particle number.

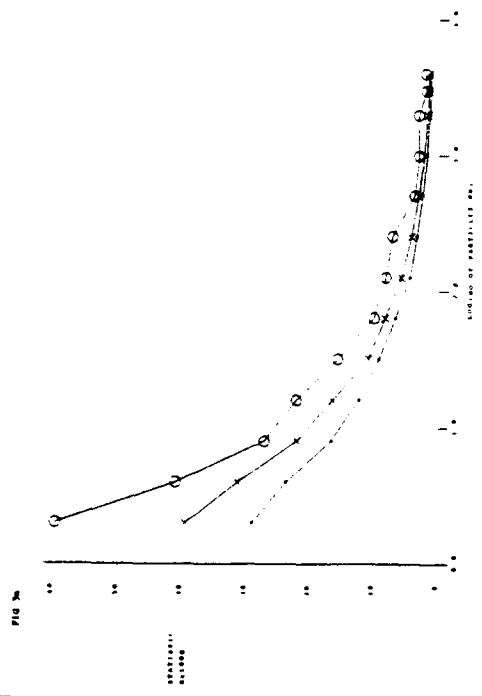
Fig.6. Exp.C: average number of particles in validation grid-cells not reached by trials, plotted against log of particle number.

Fig.7. Exp.B: Proportionate decrease in error with particle number, S_1 , defined as in (10), plotted against log of mean of n and $n+1$.

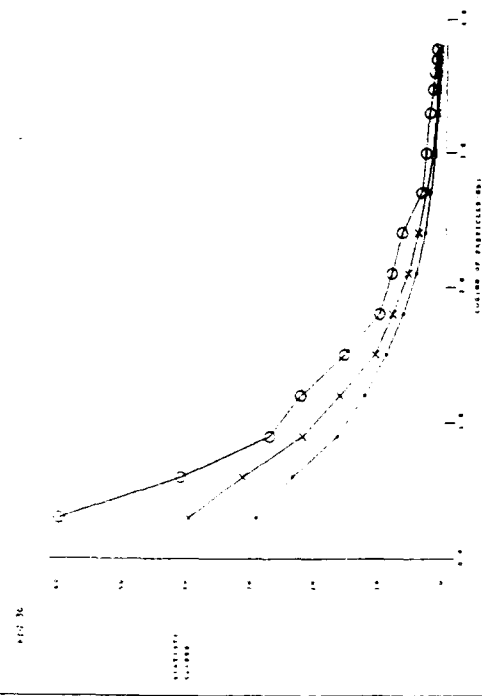
Fig.8. Exp.B: Proportionate decrease of error S_2 , defined as in (11), plotted against log of mean of n and q .



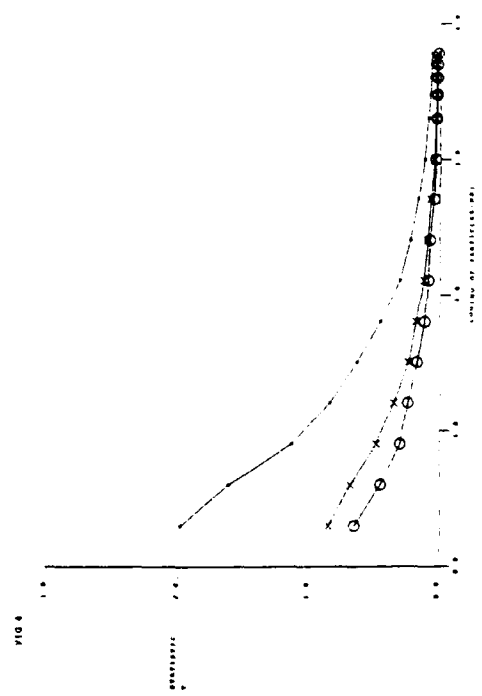
EXPERIMENT A: 4000 PAR/HR



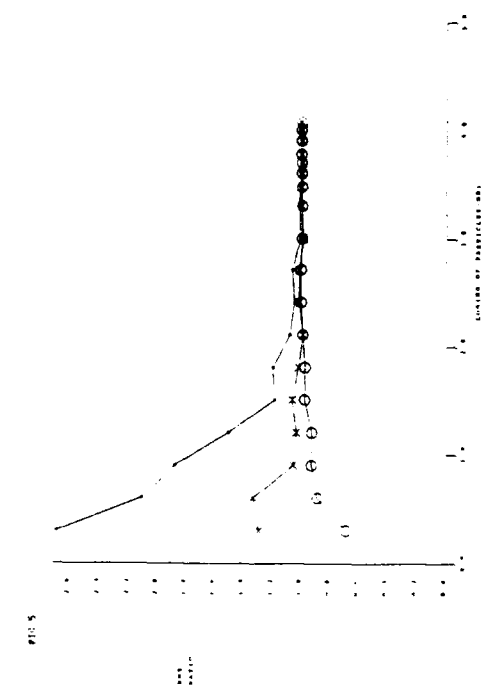
EXPERIMENT B: 6000 PAR/HR



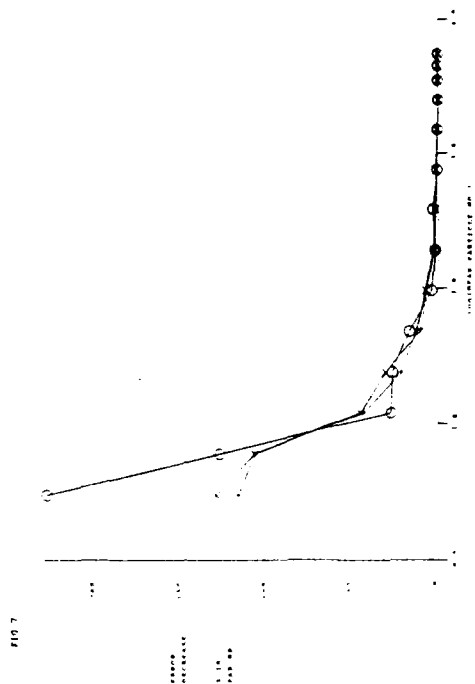
EXPERIMENT B: 6000 PAR/HR



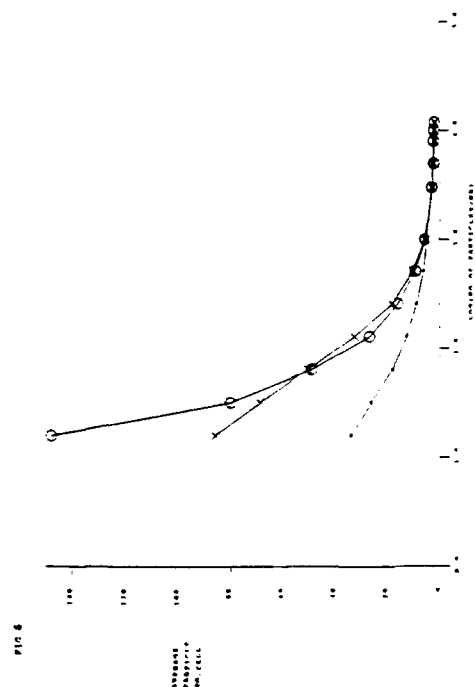
EXPERIMENT C: 12000 PAR/HR



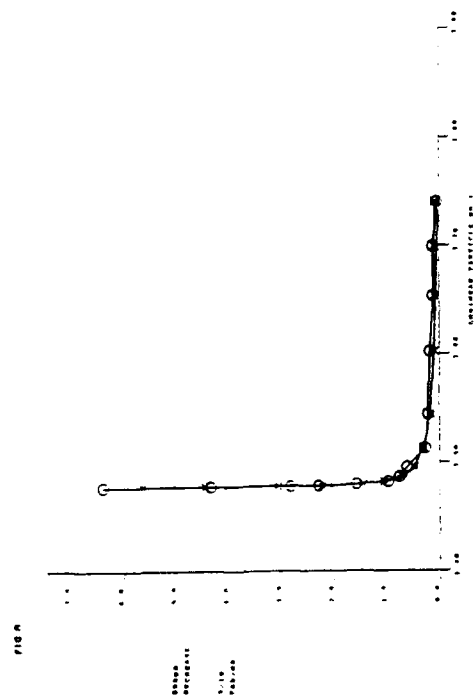
EXPERIMENT B 6000 PAR/HR



EXPERIMENT C 12000 PAR/HR



EXPERIMENT B 6000 PAR/HR



Model Intercomparison of the Kuwait Smoke Plume

A meeting held at the Meteorological Office, Bracknell 5th November 1991

R. Maryon¹, H. ApSimon² and I.M. Lowles²

1 *The Meteorological Office, London Road, Bracknell, Berkshire, RG12 2SZ, UK*

2 *Imperial College of Science, Technology and Medicine, London, SW7 2AZ, UK*

Following the ARATS 2 meeting (16-17 September 1991) Imperial College and the Meteorological Office have agreed to study the dispersion and deposition of the Kuwaiti smoke plume using two different Lagrangian multiparticle models, namely 3-DRAW (Imperial College) and NAME (Met. Office). Both organisations have agreed on the following model input data:

1. Source Positions:

- a). 29.25 N 47.40 E (derived from two sources at 29.3 N 47.6 E and 29.2 N 47.2 E)
- b). 30.50 N - 47.80 E

2. Source Terms:

The source located at position a). released 3.95×10^6 tons of Carbon per year

The source located at position b). released 6.58×10^5 tons of Carbon per year

3. Release Heights:

There are to be two release heights, one between 1000-2000 m (900-800 mb) representing an elevated release and a second between ground-level and 1000 m (1000-900 mb) corresponding to a release within the boundary layer.

4. Release Details:

The release will start at 00 GMT 27/3/91 and will continue for 48 hours.

The models will release 500 particles per hour over the same 48 hour period (00 GMT 27/3/91-00 GMT 29/3/91).

5. Meteorological Data:

Both 3-DRAW and NAME utilise meteorological fields derived from the Met. Office numerical weather prediction model FINE MESH. This model covers the area 11.25 W to 109.6875 E and from 4.5 N to 54.0 N with 129 x 67 grid points at intervals of 0.9375 degrees longitude and 0.75 degrees latitude. The horizontal components of the windfield are calculated on a wind grid offset half a cell from that described above. However, vertical wind velocities, temperature profiles, cloud cover and rainfall data are all calculated on the model grid.

FINE MESH model data will be supplied, by the Met. Office, for the period 00 GMT 27/3/91 to 00 GMT 29/3/91.

6. Model Outputs:

The models will compare the following results for 1200 GMT 28-29/3/91.

- i. *Trajectory end-points.*
- ii. *Ground and elevated level concentrations.*
- iii. *Deposition.*

Vertical concentration profiles of the smoke at 29 N 48 E on the 28/3/91 will be calculated and compared with airborne measurements performed by the Met. Office flight.

7. Timetable:

Meteorological data supplied by the Met. Office - end of November 1991

Initial model runs - end of January 1992

Revision and fine tuning - end of February 1992

Report - March 1992.